8-7-2008

Multijet Cross Sections in Charged Current e±p Scattering at HERA

S. Chekanov
Argonne National Laboratory

M. Derrick
Argonne National Laboratory

S. Magill
Argonne National Laboratory

B. Musgrave
Argonne National Laboratory

D. Nicholass
Argonne National Laboratory

See next page for additional authors

DESY–08–024
February 2008

Multi-jet cross sections in charged current $e^{\pm}p$ scattering at HERA

ZEUS Collaboration

Abstract

Jet cross sections were measured in charged current deep inelastic $e^{\pm}p$ scattering at high boson virtualities Q^2 with the ZEUS detector at HERA II using an integrated luminosity of 0.36 fb^{-1}. Differential cross sections are presented for inclusive-jet production as functions of Q^2, Bjorken x and the jet transverse energy and pseudorapidity. The dijet invariant mass cross section is also presented. Observation of three- and four-jet events in charged-current $e^{\pm}p$ processes is reported for the first time. The predictions of next-to-leading-order (NLO) QCD calculations are compared to the measurements. The measured inclusive-jet cross sections are well described in shape and normalization by the NLO predictions. The data have the potential to constrain the u and d valence quark distributions in the proton if included as input to global fits.

The ZEUS Collaboration

S. Chekanov, M. Derrick, S. Magill, B. Musgrave, D. Nicholass[1], J. Repond, R. Yoshida
Argonne National Laboratory, Argonne, Illinois 60439-4815, USA [n]

M.C.K. Mattingly
Andrews University, Berrien Springs, Michigan 49104-0380, USA

M. Jechow, N. Pavel †
Institut für Physik der Humboldt-Universität zu Berlin, Berlin, Germany [b]

P. Antonioli, G. Bari, L. Bellagamba, D. Boscherini, A. Bruni, G. Bruni, F. Cindolo, M. Corradi, G. Iacobucci, A. Margotti, R. Nania, A. Polini
INFN Bologna, Bologna, Italy [e]

S. Antonelli, M. Basile, M. Bindi, L. Cifarelli, A. Contin, S. De Pasquale[2], G. Sartorelli, A. Zichichi
University and INFN Bologna, Bologna, Italy [e]

D. Bartsch, I. Brock, H. Hartmann, E. Hilger, H.-P. Jakob, M. Jüngst, A.E. Nuncio-Quiroz, E. Paul[3], R. Renner[4], U. Samson, V. Schönberg, R. Shehzadi, M. Wlasenko
Physikalisches Institut der Universität Bonn, Bonn, Germany [b]

N.H. Brook, G.P. Heath, J.D. Morris
H.H. Wills Physics Laboratory, University of Bristol, Bristol, United Kingdom [m]

M. Capua, S. Fazio, A. Mastroberardino, M. Schioppa, G. Susinno, E. Tassi
Calabria University, Physics Department and INFN, Cosenza, Italy [e]

J.Y. Kim[5]
Chonnam National University, Kwangju, South Korea

Z.A. Ibrahim, B. Kamaluddin, W.A.T. Wan Abdullah
Jabatan Fizik, Universiti Malaya, 50603 Kuala Lumpur, Malaysia [r]

Y. Ning, Z. Ren, F. Sciulli
Nevis Laboratories, Columbia University, Irvington on Hudson, New York 10027 [o]

J. Chwastowski, A. Eskreys, J. Figiel, A. Galas, M. Gil, K. Olkiewicz, P. Stopa, L. Zawiejski
The Henryk Niewodniczanski Institute of Nuclear Physics, Polish Academy of Sciences, Cracow, Poland [i]

L. Adamczyk, T. Bołd, I. Grabowska-Bołd, D. Kisielewska, J. Łukasik, M. Przybycień, L. Suszycki
Faculty of Physics and Applied Computer Science, AGH-University of Science and Technology, Cracow, Poland [p]

A. Kotański[6], W. Słomiński[7]
Department of Physics, Jagellonian University, Cracow, Poland

U. Behrens, C. Blohm, A. Bonato, K. Borras, R. Ciesielski, N. Coppola, V. Drugakov, S. Fang, J. Fourletova[8], A. Geiser, P. Göttlicher[9], J. Grebenyuk, I. Gregor, T. Haas, W. Hain, A. Hüttmann, F. Januschek, B. Kahle, I.I. Katkov, U. Klein[10], U. Kötz[3], H. Kowalski, E. Lobodzinska, B. Löhr[3], R. Mankel, I.-A. Melzer-Pellmann, S. Miglioranzi, A. Montanari, T. Namsoo, D. Notz[11], A. Parenti, L. Rinaldi[12], P. Roloff, I. Rubinsky, R. Santamarta[13], U. Schneekloth, A. Spiridonov[14], D. Szuba[15], J. Szuba[16], T. Theedt, G. Wolf[3], K. Wrona, A.G. Yagües Molina, C. Youngman, W. Zeuner[11]
Deutsches Elektronen-Synchrotron DESY, Hamburg, Germany

V. Drugakov, W. Lohmann, S. Schlenstedt
Deutsches Elektronen-Synchrotron DESY, Zeuthen, Germany

G. Barbagli, E. Gallo
INFN Florence, Florence, Italy [e]

P. G. Pelfer
University and INFN Florence, Florence, Italy [e]

A. Bamberger, D. Dobur, F. Karstens, N.N. Vlasov[17]
Fakultät für Physik der Universität Freiburg i.Br., Freiburg i.Br., Germany [b]

P.J. Bussey[18], A.T. Doyle, W. Dunne, M. Forrest, M. Rosin, D.H. Saxon, I.O. Skillicorn
Department of Physics and Astronomy, University of Glasgow, Glasgow, United Kingdom [m]

I. Gialas[19], K. Papageorgiu
Department of Engineering in Management and Finance, Univ. of Aegean, Greece

U. Holm, R. Klanner, E. Lohrmann, P. Schleper, T. Schörner-Sadenius, J. Sztuk, H. Stadie, M. Turcato
Hamburg University, Institute of Exp. Physics, Hamburg, Germany [b]

C. Foudas, C. Fry, K.R. Long, A.D. Tapper
Imperial College London, High Energy Nuclear Physics Group, London, United Kingdom [m]

T. Matsumoto, K. Nagano, K. Tokushuku[20], S. Yamada, Y. Yamazaki[21]
Institute of Particle and Nuclear Studies, KEK, Tsukuba, Japan [f]

A.N. Barakbaev, E.G. Boos[3], N.S. Pokrovskiy, B.O. Zhautykov
Institute of Physics and Technology of Ministry of Education and Science of Kazakhstan, Almaty, Kazakhstan

V. Aushev[22], M. Borodin, A. Kozulia, M. Lisovyi
Institute for Nuclear Research, National Academy of Sciences, Kiev and Kiev National University, Kiev, Ukraine

D. Son
Kyungpook National University, Center for High Energy Physics, Daegu, South Korea [g]

J. de Favereau, K. Piotrzkowski
Institut de Physique Nucléaire, Université Catholique de Louvain, Louvain-la-Neuve, Belgium [q]

F. Barreiro, C. Glasman, M. Jimenez, L. Labarga, J. del Peso, E. Ron, M. Soares, J. Terrón, M. Zambrana
Departamento de Física Teórica, Universidad Autónoma de Madrid, Madrid, Spain [l]

F. Corriveau, C. Liu, J. Schwartz, R. Walsh, C. Zhou
Department of Physics, McGill University, Montréal, Québec, Canada H3A 2T8 [a]

T. Tsurugai
Meiji Gakuin University, Faculty of General Education, Yokohama, Japan [f]

A. Antonov, B.A. Dolgoshein, D. Gladkov, V. Sosnovtsev, A. Stifutkin, S. Suchkov
Moscow Engineering Physics Institute, Moscow, Russia [j]

R.K. Dementiev, P.F. Ermolov, L.K. Gladilin, Yu.A. Golubkov, L.A. Khein, I.A. Korzhavina, V.A. Kuzmin, B.B. Levchenko[23], O.Yu. Lukina, A.S. Proskuryakov, L.M. Shcheglova, D.S. Zotkin
Moscow State University, Institute of Nuclear Physics, Moscow, Russia [k]

I. Abt, C. Büttner, A. Caldwell, D. Kollar, B. Reisert, W.B. Schmidke, J. Sutiak
Max-Planck-Institut für Physik, München, Germany

G. Grigorescu, A. Keramidas, E. Koffeman, P. Kooijman, A. Pellegrino, H. Tiecke, M. Vázquez[11], L. Wiggers
NIKHEF and University of Amsterdam, Amsterdam, Netherlands [h]

N. Brümmer, B. Bylsma, L.S. Durkin, A. Lee, T.Y. Ling
Physics Department, Ohio State University, Columbus, Ohio 43210 [n]

P.D. Allfrey, M.A. Bell, A.M. Cooper-Sarkar, R.C.E. Devenish, J. Ferrando, B. Foster, K. Korcsak-Gorzo, K. Oliver, S. Patel, V. Roberfroid[24], A. Robertson, P.B. Straub, C. Uribe-Estrada, R. Walczak
Department of Physics, University of Oxford, Oxford United Kingdom [m]

A. Bertolin, F. Dal Corso, S. Dusini, A. Longhin, L. Stanco
INFN Padova, Padova, Italy [e]

P. Bellan, R. Brugnera, R. Carlin, A. Garfagnini, S. Limentani
Dipartimento di Fisica dell' Università and INFN, Padova, Italy [e]

B.Y. Oh, A. Raval, J. Ukleja[25], J.J. Whitmore[26]
Department of Physics, Pennsylvania State University, University Park, Pennsylvania 16802 [o]

Y. Iga
Polytechnic University, Sagamihara, Japan [f]

G. D'Agostini, G. Marini, A. Nigro
Dipartimento di Fisica, Università 'La Sapienza' and INFN, Rome, Italy [e]

J.E. Cole, J.C. Hart
Rutherford Appleton Laboratory, Chilton, Didcot, Oxon, United Kingdom [m]

H. Abramowicz[27], A. Gabareen, R. Ingbir, S. Kananov, A. Levy, O. Smith, A. Stern
Raymond and Beverly Sackler Faculty of Exact Sciences, School of Physics, Tel-Aviv University, Tel-Aviv, Israel [d]

M. Kuze, J. Maeda
Department of Physics, Tokyo Institute of Technology, Tokyo, Japan [f]

R. Hori, S. Kagawa[28], N. Okazaki, S. Shimizu, T. Tawara
Department of Physics, University of Tokyo, Tokyo, Japan [f]

R. Hamatsu, H. Kaji[29], S. Kitamura[30], O. Ota, Y.D. Ri
Tokyo Metropolitan University, Department of Physics, Tokyo, Japan [f]

M. Costa, M.I. Ferrero, V. Monaco, R. Sacchi, A. Solano
Università di Torino and INFN, Torino, Italy [e]

M. Arneodo, M. Ruspa
Università del Piemonte Orientale, Novara, and INFN, Torino, Italy [e]

S. Fourletov[8], J.F. Martin, T.P. Stewart
Department of Physics, University of Toronto, Toronto, Ontario, Canada M5S 1A7 [a]

S.K. Boutle[19], J.M. Butterworth, C. Gwenlan[31], T.W. Jones, J.H. Loizides, M. Wing[32]
Physics and Astronomy Department, University College London, London, United Kingdom [m]

B. Brzozowska, J. Ciborowski[33], G. Grzelak, P. Kulinski, P. Łużniak[34], J. Malka[34], R.J. Nowak, J.M. Pawlak, T. Tymieniecka, A. Ukleja, A.F. Żarnecki
Warsaw University, Institute of Experimental Physics, Warsaw, Poland

M. Adamus, P. Plucinski[35]
Institute for Nuclear Studies, Warsaw, Poland

Y. Eisenberg, D. Hochman, U. Karshon
Department of Particle Physics, Weizmann Institute, Rehovot, Israel [c]

E. Brownson, T. Danielson, A. Everett, D. Kçira, D.D. Reeder[3], P. Ryan, A.A. Savin, W.H. Smith, H. Wolfe
Department of Physics, University of Wisconsin, Madison, Wisconsin 53706, USA [n]

S. Bhadra, C.D. Catterall, Y. Cui, G. Hartner, S. Menary, U. Noor, J. Standage, J. Whyte
Department of Physics, York University, Ontario, Canada M3J 1P3 [a]

[1] also affiliated with University College London, UK
[2] now at University of Salerno, Italy
[3] retired
[4] now at Bruker AXS, Karlsruhe, Germany
[5] supported by Chonnam National University in 2006
[6] supported by the research grant no. 1 P03B 04529 (2005-2008)
[7] This work was supported in part by the Marie Curie Actions Transfer of Knowledge project COCOS (contract MTKD-CT-2004-517186)
[8] now at University of Bonn, Germany
[9] now at DESY group FEB, Hamburg, Germany
[10] now at University of Liverpool, UK
[11] now at CERN, Geneva, Switzerland
[12] now at Bologna University, Bologna, Italy
[13] now at BayesForecast, Madrid, Spain
[14] also at Institut of Theoretical and Experimental Physics, Moscow, Russia
[15] also at INP, Cracow, Poland
[16] also at FPACS, AGH-UST, Cracow, Poland
[17] partly supported by Moscow State University, Russia
[18] Royal Society of Edinburgh, Scottish Executive Support Research Fellow
[19] also affiliated with DESY, Germany
[20] also at University of Tokyo, Japan
[21] now at Kobe University, Japan
[22] supported by DESY, Germany
[23] partly supported by Russian Foundation for Basic Research grant no. 05-02-39028-NSFC-a
[24] EU Marie Curie Fellow
[25] partially supported by Warsaw University, Poland
[26] This material was based on work supported by the National Science Foundation, while working at the Foundation.
[27] also at Max Planck Institute, Munich, Germany, Alexander von Humboldt Research Award
[28] now at KEK, Tsukuba, Japan
[29] now at Nagoya University, Japan
[30] Department of Radiological Science, Tokyo Metropolitan University, Japan
[31] PPARC Advanced fellow
[32] also at Hamburg University, Inst. of Exp. Physics, Alexander von Humboldt Research Award and partially supported by DESY, Hamburg, Germany
[33] also at Łódź University, Poland
[34] Łódź University, Poland

[35] now at Lund Universtiy, Lund, Sweden

[†] deceased

[a] supported by the Natural Sciences and Engineering Research Council of Canada (NSERC)

[b] supported by the German Federal Ministry for Education and Research (BMBF), under contract numbers 05 HZ6PDA, 05 HZ6GUA, 05 HZ6VFA and 05 HZ4KHA

[c] supported in part by the MINERVA Gesellschaft für Forschung GmbH, the Israel Science Foundation (grant no. 293/02-11.2) and the U.S.-Israel Binational Science Foundation

[d] supported by the German-Israeli Foundation and the Israel Science Foundation

[e] supported by the Italian National Institute for Nuclear Physics (INFN)

[f] supported by the Japanese Ministry of Education, Culture, Sports, Science and Technology (MEXT) and its grants for Scientific Research

[g] supported by the Korean Ministry of Education and Korea Science and Engineering Foundation

[h] supported by the Netherlands Foundation for Research on Matter (FOM)

[i] supported by the Polish State Committee for Scientific Research, grant no. 620/E-77/SPB/DESY/P-03/DZ 117/2003-2005 and grant no. 1P03B07427/2004-2006

[j] partially supported by the German Federal Ministry for Education and Research (BMBF)

[k] supported by RF Presidential grant N 8122.2006.2 for the leading scientific schools and by the Russian Ministry of Education and Science through its grant for Scientific Research on High Energy Physics

[l] supported by the Spanish Ministry of Education and Science through funds provided by CICYT

[m] supported by the Science and Technology Facilities Council, UK

[n] supported by the US Department of Energy

[o] supported by the US National Science Foundation. Any opinion, findings and conclusions or recommendations expressed in this material are those of the authors and do not necessarily reflect the views of the National Science Foundation.

[p] supported by the Polish Ministry of Science and Higher Education as a scientific project (2006-2008)

[q] supported by FNRS and its associated funds (IISN and FRIA) and by an Inter-University Attraction Poles Programme subsidised by the Belgian Federal Science Policy Office

[r] supported by the Malaysian Ministry of Science, Technology and Innovation/Akademi Sains Malaysia grant SAGA 66-02-03-0048

1 Introduction

Jet production in charged-current (CC) deep inelastic $e^{\pm}p$ scattering (DIS) provides a testing ground for QCD and for the electroweak sector of the Standard Model (SM). Up to leading order (LO) in the strong coupling constant, α_s, jet production in CC DIS proceeds via the quark-parton model ($Wq \to q$, Fig. 1a), W-gluon fusion ($Wg \to q\bar{q}$, Fig. 1b) and the QCD-Compton ($Wq \to qg$, Fig. 1c) processes. Thus, differential cross sections for jet production are sensitive to both the value of α_s and the mass of the propagator, M_W, which are fundamental parameters of the theory. Cross sections in CC DIS are also sensitive to the valence flavor content of the proton, since the $W^{-(+)}$ couples to the up-like (down-like) quarks in the proton.

The large center-of-mass energy available at the HERA $e^{\pm}p$ collider ($\sqrt{s} = 318$ GeV) extends the kinematic region for studying CC DIS with respect to fixed-target neutrino scattering experiments [1] by about two orders of magnitude in the virtuality of the exchanged boson, Q^2, and to lower values of the fraction of the proton momentum carried by the struck parton, x. Measurements of the CC DIS cross section at HERA [2–4] demonstrated, at high Q^2, the presence of a space-like propagator with a finite mass, consistent with that of the W boson. During 2002–2007, HERA provided longitudinally-polarized electron or positron beams. Measurements of the fully-inclusive CC DIS cross section for positive and negative values of the longitudinal polarization of the beams were found to be in good agreement with the predictions of the SM [5, 6].

At HERA, multijet structures were observed in CC DIS [3, 7, 8] at large Q^2 and jet shapes and subjet multiplicities were measured [8, 9] and compared with neutral current (NC) DIS processes [9, 10]. The subjet multiplicities were used to extract a value of $\alpha_s(M_Z)$ [8].

In this paper, measurements are presented of inclusive-jet and dijet cross sections in CC $e^{\pm}p$ DIS in the laboratory frame. Measurements of three-jet differential cross sections in CC DIS were measured for the first time in $e^{\pm}p$ collisions. A small sample of four-jet events was also observed in the data. The measurements are presented as functions of Q^2, x, the jet transverse energy, $E_T^{\rm jet}$, and pseudorapidity[1], $\eta^{\rm jet}$, and as a function of the invariant mass of the jet system in dijet and three-jet events. Predictions from next-to-leading-order (NLO) QCD calculations are compared to the measurements. Results for negative and positive longitudinally-polarized electron and positron beams are also presented.

[1] The ZEUS coordinate system is a right-handed Cartesian system, with the Z axis pointing in the proton beam direction, referred to as the "forward direction", and the X axis pointing left towards the center of HERA. The coordinate origin is at the nominal interaction point.

2 Experimental set-up

A detailed description of the ZEUS detector can be found elsewhere [11, 12]. A brief outline of the components most relevant for this analysis is given below.

Charged particles were tracked in the central tracking detector (CTD) [13], which operated in a magnetic field of 1.43 T provided by a thin superconducting solenoid. The CTD consisted of 72 cylindrical drift-chamber layers, organized in nine superlayers covering the polar-angle region $15^\circ < \theta < 164^\circ$. In 2001, a silicon microvertex detector (MVD) [14] was installed between the beampipe and the inner radius of the CTD. The MVD was organized into a barrel with three cylindrical layers and a forward section with four planar layers perpendicular to the HERA beam direction. The barrel contained 600 single-sided silicon strip sensors each having 512 strips of width 120 μm; the forward section contained 112 sensors each of which had 480 strips of width 120 μm. Charged-particle tracks were reconstructed online by using the ZEUS global tracking trigger [15], which combined information from the CTD and MVD. The online tracks were used to reconstruct the interaction vertex and reject non-ep background. Offline, the tracks used in this analysis were reconstructed using information from the CTD and were used, in addition to the vertex reconstruction, to cross-check the energy scale of the calorimeter.

The high-resolution uranium–scintillator calorimeter (CAL) [16] covered 99.7% of the total solid angle and consisted of three parts: the forward (FCAL), the barrel (BCAL) and the rear (RCAL) calorimeters. Each part was subdivided transversely into towers and longitudinally into one electromagnetic section (EMC) and either one (in RCAL) or two (in BCAL and FCAL) hadronic sections (HAC). The smallest subdivision of the calorimeter is called a cell. Under test-beam conditions, the CAL single-particle relative energy resolutions were $\sigma(E)/E = 0.18/\sqrt{E}$ for leptons and $\sigma(E)/E = 0.35/\sqrt{E}$ for hadrons, with E in GeV.

The luminosity was measured using the Bethe-Heitler reaction $ep \to e\gamma p$ by the luminosity detector which consisted of two independent systems. In the first system, the photons were detected by a lead-scintillator calorimeter placed in the HERA tunnel 107 m from the interaction point in the lepton-beam direction. The system used in previous ZEUS publications [17] was modified by the addition of active filters in order to suppress the increased synchrotron radiation background of the upgraded HERA collider. The second system was a magnetic spectrometer arrangement [18], which measured electron-positron pairs from converted photons. The fractional uncertainty on the measured luminosity was 3.5%.

The lepton beam in HERA became transversely polarized naturally through the Sokolov-Ternov effect [19], with a build-up time of approximately 40 minutes. Spin rotators on either side of the ZEUS detector changed the transverse polarization of the beam

into longitudinal polarization. The lepton-beam polarization was measured using two independent polarimeters, the transverse polarimeter (TPOL) [20,21] and the longitudinal polarimeter (LPOL) [21, 22]. Both devices exploited the spin-dependent cross section for Compton scattering of circularly polarized photons off leptons to measure the beam polarization. The fractional uncertainty on the measured polarization was 4.2% and 3.6% from TPOL and LPOL, respectively.

3 Data selection and jet search

The data were collected from 2004 to 2007, when HERA operated with protons of energy $E_p = 920$ GeV and electrons (positrons) of energy $E_e = 27.5$ GeV, and correspond to an integrated luminosity of 180.0 ± 6.3 (178.5 ± 6.2) pb^{-1}. Samples of negatively- (positively-) polarized electron beams with an integrated luminosity of 106.4 (73.6) pb^{-1} and luminosity-weighted average polarization of $P_{e^-}^{\rm neg} = -0.27 \pm 0.01$ ($P_{e^-}^{\rm pos} = +0.29 \pm 0.01$) were analyzed. For positrons, the samples analyzed were of 76.5 and 102.1 pb^{-1} with a luminosity-weighted average polarization of $P_{e^+}^{\rm neg} = -0.37^{+0.01}_{-0.02}$ and $P_{e^+}^{\rm pos} = +0.32 \pm 0.01$, respectively.

The main signature of a CC DIS event at HERA is the presence of large $p_T^{\rm miss}$ and large $E_T^{\rm tot}$, where $p_T^{\rm miss}$ is the missing transverse momentum arising from the energetic final-state neutrino which escapes detection and $E_T^{\rm tot}$ is the total transverse energy arising from the hard interaction. The variable $p_T^{\rm miss}$ was reconstructed using the vectorial sum $p_T^{\rm miss} = \sqrt{(\sum_i p_{X,i})^2 + (\sum_i p_{Y,i})^2}$ and $E_T^{\rm tot}$ was reconstructed as the scalar sum $E_T^{\rm tot} = \sum_i E_{T,i}$. In both cases, the sum runs over all CAL cells. The online selection of the signal was based on the ZEUS three-level trigger [12]. Two different trigger selections were used. One trigger selection relied on large $p_T^{\rm miss}$ and large $E_T^{\rm tot}$. The alternative trigger selection additionally required the presence of at least one jet with transverse energy above 8 GeV. Events from CC DIS interactions were selected offline using criteria similar to those of an earlier publication [8]. The kinematic variables Q^2, the inelasticity, y, and x were estimated using the method of Jacquet-Blondel [23], which uses the information from the hadronic energy flow of the event, and corrected for detector effects as described elsewhere [9, 24]. These estimators were reconstructed as:

$$y_{\rm JB} = \frac{\sum_i (E_i - p_{Z,i})}{2\ E_e}, \qquad Q^2_{\rm JB} = \frac{(p_T^{\rm miss})^2}{1 - y_{\rm JB}} \qquad \text{and} \qquad x_{\rm JB} = \frac{Q^2_{\rm JB}}{s\ y_{\rm JB}},$$

where the sum runs over all CAL cells. The main selection criteria were:

- $p_T^{\rm miss} > 11$ GeV;
- $p_T^{\rm miss}/E_T^{\rm tot} > 0.5$, to reject photoproduction and beam-gas background;

- the vertex position along the beam axis in the range $-35 < Z_{\rm vtx} < 33$ cm, consistent with an $e^{\pm}p$ interaction;
- at least one track associated with the vertex, which had a polar angle between 15° and 164° and a transverse momentum exceeding 0.15 GeV, to reject non-$e^{\pm}p$ background;
- $|\Delta\varphi| < 1$ rad, where $|\Delta\varphi|$ is the difference between the azimuth of the net transverse momentum as measured by the tracks associated with the vertex and the azimuth measured by the CAL. This requirement reduced the contamination from random coincidences of cosmic rays with $e^{\pm}p$ interactions;
- $P_{T,\rm tracks}/p_T^{\rm miss} > 0.1$, where $P_{T,\rm tracks}$ is the net transverse momentum of the tracks associated with the vertex (this condition was not applied if $p_T^{\rm miss} > 25$ GeV). This cut rejected events with additional energy deposits in the CAL not related to $e^{\pm}p$ interactions (mainly cosmic rays) and beam-related background in which $p_T^{\rm miss}$ has a small polar angle;
- events were removed from the sample if there was an isolated electron or positron candidate with energy above 10 GeV, to reject NC DIS events;
- events were rejected if $E_{\rm BHAC2}/E_{\rm BCAL} > 0.5$ for $E_{\rm BCAL} > 2$ GeV and $E_{\rm BHAC1}/E_{\rm BCAL} > 0.85$ for $E_{\rm BCAL} > 8$ GeV, where $E_{\rm BHAC1(BHAC2)}$ is the energy deposited in the first (second) HAC section of BCAL and $E_{\rm BCAL}$ is the total energy deposition in BCAL. These requirements rejected beam-related background;
- tracking requirements were not applied if the highest-$E_T^{\rm jet}$ jet (see below) in the event had $\eta^{\rm jet} > 2$; in such a case, a tighter $p_T^{\rm miss}$ cut of 20 GeV was applied;
- $Q^2 > 200$ GeV^2, to ensure high trigger efficiency;
- $y < 0.9$, to avoid the degradation of the resolution in Q^2 near $y \sim 1$.

The selected events were visually inspected and a few remaining non-$e^{\pm}p$ background events (1.2% of the final sample), mainly cosmic-ray and halo-muon events, were removed.

Jets were identified in the pseudorapidity (η) - azimuth (ϕ) plane of the laboratory frame using the k_T cluster algorithm [25] in the longitudinally invariant inclusive mode [26]. This algorithm combines objects with a small relative distance d_{ij},

$$d_{ij} = \min(E_{T,i}, E_{T,j})^2 \cdot ((\eta_i - \eta_j)^2 + (\phi_i - \phi_j)^2),$$

where $E_{T,i}$, η_i and ϕ_i are the transverse energy, pseudorapidity and azimuth of object i. The axis of the jet was defined according to the Snowmass convention [27], where $\eta^{\rm jet}$ ($\phi^{\rm jet}$) is the transverse-energy weighted mean pseudorapidity (azimuth) of all the objects belonging to that jet. The jets were reconstructed using the CAL and corrected [24, 28] for detector effects to yield jets of hadrons. Events with at least one jet in the range

$-1 < \eta^{\rm jet} < 2.5$ were retained. The inclusive-jet sample contained $N^{\rm neg} = 5335$ (870) and $N^{\rm pos} = 2122$ (2284) jets with $E_T^{\rm jet} > 14$ GeV in the e^-p (e^+p) data, where $N^{\rm neg(pos)}$ is the number of jets selected in events with negatively-(positively-)polarized lepton beams. The dijet sample was selected requiring the jets with the highest and second-highest $E_T^{\rm jet}$ to have $E_T^{\rm jet1} > 14$ and $E_T^{\rm jet2} > 5$ GeV, respectively. The three-jet sample was selected from the dijet sample by requiring the third-highest $E_T^{\rm jet}$ jet to have $E_T^{\rm jet3} > 5$ GeV. The e^-p (e^+p) dijet and three-jet samples contained 1117 (464) and 109 (30) events, respectively. Eleven events contained a fourth jet with $E_T^{\rm jet} > 5$ GeV.

4 Monte Carlo simulation

Samples of Monte Carlo (MC) events were generated to determine the response of the detector and to evaluate the correction factors necessary to obtain the hadron-level jet cross sections. The hadron level is defined by those hadrons with lifetime $\tau \geq 10$ ps. The generated events were passed through the GEANT 3.21-based [29] ZEUS detector- and trigger-simulation programs [12]. They were reconstructed and analyzed by the same program chain as the data. The CC DIS events were generated using the LEPTO 6.5 program [30] interfaced to HERACLES 4.6.1 [31] via DJANGOH 1.3 [32]. The HERACLES program includes first-order electroweak radiative corrections, vertex and propagator terms, and two-boson exchange. The CTEQ5D [33] proton parton distribution functions (PDFs) were used. The QCD radiation was modeled with the color-dipole model (CDM) [34] by using the ARIADNE 4.08 program [35] including the boson-gluon-fusion process. To study the systematic effect of the modeling of parton showers in the correction of the data, samples of events were generated using the LEPTO model which is based on first-order QCD matrix elements and parton showers (MEPS). For the generation of the LEPTO-MEPS samples[2], the option for soft-color interactions was switched off. In both cases, fragmentation into hadrons was performed using the Lund string model [36] as implemented in JETSET 7.4 [37, 38].

The photoproduction background was estimated using resolved and direct samples generated using the program HERWIG 5.9 [39]. After all the selection cuts described in the previous section, the contribution from photoproduction events to the inclusive-jet sample was estimated to be smaller than 0.5% overall and amounted to $\sim 2\%$ in the lowest $E_T^{\rm jet}$ bin. The NC DIS contamination was estimated to be smaller than the photoproduction background. No background subtraction was performed.

[2] The program LEPTO allows the generation of only QPM events when using the MEPS option for e^-p collisions; thus, only positron samples were generated and used as an estimate of the systematic effect also for e^-p collisions.

The jet search was performed on the MC events using the energy measured in the CAL cells in the same way as for the data. The MC samples provided a good description of the measured distributions of the kinematic and jet variables. The data distributions as functions of $\eta^{\rm jet}$, $E_T^{\rm jet}$, Q^2 and x for the inclusive-jet samples are shown in Figs. 2 (e^-p) and 3 (e^+p) separately for negatively- and positively-polarized electron and positron beams. Figure 4 shows the $\eta^{\rm jet1}$, $\eta^{\rm jet2}$, $E_T^{\rm jet1}$ and $E_T^{\rm jet2}$ distributions for the dijet sample. These figures also show the MC simulations normalized to the number of jets in the data.

The same jet algorithm was also applied to the final-state hadrons to obtain the predictions at the hadron level. To correct the data to the hadron level, multiplicative correction factors, defined as ratios of the measured quantities for jets (events) of hadrons over the same quantity for jets (events) at detector level, were estimated by using the CDM samples and applied to the inclusive-jet (dijet and three-jet) data distributions. The samples of LEPTO-MEPS were used as an estimation of the uncertainty on the modeling of the parton shower.

Parton-level predictions were also obtained by applying the jet algorithm to the MC-generated partons. These predictions were used to correct the fixed-order QCD calculations (see Section 5) to the hadron level. The program HERACLES was used to correct the predicted cross sections to the electroweak Born level evaluated using the fine structure constant $\alpha = 1/137.035999$, the Fermi coupling constant $G_F = 1.1664 \cdot 10^{-5}$ GeV^{-2} and the mass of the Z boson $M_Z = 91.1876$ GeV to determine the electroweak parameters.

5 Fixed-order QCD calculations

Fixed-order QCD calculations were obtained using the program MEPJET [40], which employs the phase-space slicing method [41]. This is the only available program providing fixed-order QCD calculations for jet production in CC DIS. The jet algorithm described in Section 3 was also applied to the partons in the events generated by MEPJET to compute the predictions for the jet cross sections. The calculations were performed in the $\overline{\rm MS}$ scheme. The calculations are $\mathcal{O}(\alpha_s)$ ($\mathcal{O}(\alpha_s^2)$) for inclusive-jet (dijet and three-jet) production; this means that for inclusive-jet and dijet cross sections, the predictions are NLO whereas those for three-jet cross sections are only LO. The number of flavors was set to five and the renormalization (μ_R) and factorization (μ_F) scales were chosen to be $\mu_R = \mu_F = Q$. The calculations were performed using the ZEUS-S [42] parameterizations of the proton PDFs. Alternative calculations were performed using the CTEQ6 [43] and MRST2001 [44] sets of proton PDFs. The cross sections were evaluated using the same values for α, G_F and M_Z as in the MC simulations (Section 4). The mass of the W boson was fixed to 80.40 GeV [45]. The strong coupling constant was calculated at two loops

with $\Lambda^{(5)}_{\overline{\rm MS}} = 226$ MeV, corresponding to $\alpha_s(M_Z) = 0.118$.

Since the measurements correspond to jets of hadrons whereas the QCD calculations correspond to jet of partons, the predictions were corrected to the hadron level using MC simulations. The multiplicative correction factor ($C_{\rm had}$) is defined as the ratio of the cross sections for jets of hadrons to the same quantity for jets of partons, estimated using the MC programs described in Section 4. The ratios obtained with the CDM model were taken as the default corrections, whereas those from the LEPTO-MEPS model were used as an estimation of the effect of the parton shower. The value of $C_{\rm had}$ typically differs from unity by less than 5%, 10% and 30% for the inclusive-jet, dijet and three-jet cross sections, respectively.

The following sources of uncertainty in the theoretical predictions were considered:

- the uncertainty on the NLO QCD calculations due to terms beyond NLO, estimated by varying μ_R between $Q/2$ and $2Q$, was typically below $\pm 2\%$ for the inclusive-jet cross sections and below $\pm 5\%$ for the dijet cross sections. For the LO calculations of the three-jet cross sections the uncertainty was $\approx \pm 30\%$. For the three-jet cross sections, this uncertainty is dominant. Thus, no other theoretical uncertainty was taken into account for the three-jet cross sections;
- the uncertainty on the NLO QCD calculations due to those on the proton PDFs was estimated by repeating the calculations using 22 additional sets from the ZEUS-S analysis, which takes into account the statistical and correlated systematic experimental uncertainties of each data set used in the determination of the proton PDFs. The resulting uncertainty in the inclusive-jet $e^- p$ ($e^+ p$) cross sections was below ± 2 (4)%, except in the high-$E_T^{\rm jet}$, high-Q^2 and high-x regions where it reached ± 4 (10)%. The resulting uncertainty in the dijet $e^- p$ ($e^+ p$) cross sections was below ± 5 (5)%, except in the high-$E_T^{\rm jet}$, high-Q^2 and high-x regions where it reached ± 7 (15)%;
- the uncertainty on the NLO QCD calculations due to that on $\alpha_s(M_Z)$ was estimated by repeating the calculations using two additional sets of proton PDFs, for which different values of $\alpha_s(M_Z)$ were assumed in the fits. The difference between the calculations using these various sets was scaled by a factor such as to reflect the uncertainty on the current world average of α_s [46]. The resulting uncertainty in the cross sections was below $\pm 1\%$;
- the uncertainty from the modeling of the QCD cascade was estimated as the difference between the hadronization corrections obtained using the ARIADNE and LEPTO-MEPS models. The resulting uncertainty on the inclusive-jet and dijet cross sections was typically below 1%;
- the uncertainty of the calculations due to the value of μ_F was estimated by repeating the calculations with $\mu_F = Q/2$ and $2Q$. The effect was negligible.

The total theoretical uncertainty was obtained by adding the individual uncertainties listed above in quadrature.

6 Systematic uncertainties

The following sources of systematic uncertainty were considered for the measurements of the jet cross sections [24]; values in percentage of the effects for the integrated inclusive-jet, dijet and three-jet cross sections are shown in parentheses:

- the uncertainty in the absolute energy scale of the jets was estimated by studying the differences between data and MC simulation in single-jet NC DIS events [24, 47] by comparing the transverse energy imbalance between the scattered electron or positron and the jet. The uncertainty was found to be $\pm 1\%$ for $E_T^{\rm jet} < 75$ GeV and $\pm 2\%$ for $E_T^{\rm jet} > 75$ GeV (0.5%, 2%, 4%);
- the uncertainty in the reconstruction of the kinematic variables due to the uncertainty in the absolute energy scale of the CAL was estimated by varying $p_T^{\rm miss}$ and $y_{\rm JB}$ as measured with the CAL by $\pm 1\%$ for $p_T^{\rm miss} < 75$ GeV and $^{+3}_{-1}\%$ for $p_T^{\rm miss} > 75$ GeV in the MC samples (0.2%, 0.3%, 0.4%);
- the differences in the results obtained by using either CDM or LEPTO-MEPS to correct the data for detector effects were taken as systematic uncertainties due to the modeling of the parton shower (0.7%, 7%, 6%);
- the selection cut of $p_T^{\rm miss} > 11$ GeV was changed to 10 GeV and 12 GeV in data and MC events (0.2%, 0.1%, below 0.1%);
- the uncertainty in the simulation of the vertex position was estimated by changing the selection cut to $-24 < Z_{\rm vtx} < 22$ cm in data and MC events (2%, 2%, 2%);
- the uncertainty in the simulation of the trigger was estimated to be negligible by using two different trigger selections in data and MC events (see Section 3).

The experimental uncertainties are dominated by the statistical uncertainty of the data, except for the inclusive-jet differential cross sections at high $E_T^{\rm jet}$ and high Q^2, where the uncertainty coming from the modeling of the parton shower is large. The systematic uncertainties not associated with the absolute energy scale were added in quadrature to the statistical uncertainties and are shown in the figures as error bars. The uncertainties due to the absolute energy scale of the jets and the CAL were added linearly, due to the large bin-to-bin correlation, and are shown separately in the tables. In addition, there was an overall normalization uncertainty of 3.5% from the luminosity determination and $3-5\%$ uncertainty on the polarization measurement.

7 Results

7.1 Polarized inclusive-jet cross sections

Differential inclusive-jet cross sections were measured in the kinematic regime $Q^2 > 200$ GeV^2 and $y < 0.9$. The cross sections were determined for jets with $E_T^{\rm jet} > 14$ GeV and $-1 < \eta^{\rm jet} < 2.5$.

The inclusive-jet differential cross sections as functions of $\eta^{\rm jet}$, $E_T^{\rm jet}$, Q^2 and x for negatively- and positively-polarized e^-p (e^+p) collisions are shown in Fig. 5 (6) and Tables 1 to 4. The predictions of the NLO calculations are compared to the data in the figures. The lower parts of the figures show the ratio of the cross sections for negatively- and positively-polarized lepton beams, which is in agreement with the measured polarization ratio, $(1 - P_{e^-}^{\rm neg})/(1 - P_{e^-}^{\rm pos}) = 1.79 \pm 0.05$ for e^-p and $(1 + P_{e^+}^{\rm pos})/(1 + P_{e^+}^{\rm neg}) = 2.10^{+0.08}_{-0.14}$ for e^+p. The integrated polarized inclusive-jet cross sections, $\sigma_{\rm jets}$, are shown in Table 5. The measured cross sections are in good agreement with the predictions of the SM as given by the NLO QCD calculations, also shown in Table 5, in the kinematic range studied.

7.2 Unpolarized inclusive-jet cross sections

Figure 7 and Tables 6 to 13 show the unpolarized inclusive-jet differential cross sections as functions of $\eta^{\rm jet}$, $E_T^{\rm jet}$, Q^2 and x in CC $e^\pm p$ DIS. The unpolarized cross section for an observable A was obtained via

$$\frac{d\sigma}{dA}(e^\pm) = \frac{N_{\rm data}^{\rm unpol}(e^\pm)}{\mathcal{L}_{e^\pm} \cdot \Delta A} \cdot \frac{N_{\rm MC}^{\rm had}}{N_{\rm MC}^{\rm det}},$$

where

$$N_{\rm data}^{\rm unpol}(e^\pm) = \frac{N_{\rm data}^{\rm neg}(e^\pm)}{1 \pm P_{e^\pm}^{\rm neg}} + \frac{N_{\rm data}^{\rm pos}(e^\pm)}{1 \pm P_{e^\pm}^{\rm pos}},$$

$\mathcal{L}_{e^\pm}$ is the total integrated luminosity for $e^\pm p$ collisions and ΔA is the bin width.

The measured $d\sigma/d\eta^{\rm jet}$ has a maximum at $\eta^{\rm jet} \approx 1$. The measured $d\sigma/dE_T^{\rm jet}$ exhibits a fall-off of two (three) orders of magnitude in the e^-p (e^+p) sample. Values of $E_T^{\rm jet}$ of more than 100 GeV are accessible with the present statistics. For $200 < Q^2 \lesssim 2000$ GeV^2, the distributions display a weak dependence on Q^2. The cross sections as functions of $E_T^{\rm jet}$ and Q^2 show a less rapid fall-off than what is observed in NC DIS processes due to the presence of the massive W propagator. Furthermore, the measured cross sections for the e^+p sample decrease more rapidly as a function of $E_T^{\rm jet}$ and Q^2 than for the e^-p sample

(see below). The values in x accessible by the data are within the range $0.013 < x < 0.63$, as shown in Fig. 7d. The NLO QCD predictions using the ZEUS-S PDF sets are compared to the data in Fig. 7. Figure 8 shows the relative difference between the data and the predictions. The NLO QCD predictions give a reasonable description of the shape and normalization of the data.

Figure 8 also displays the ratio of the e^-p and e^+p differential cross sections. The measured ratio as a function of $\eta^{\rm jet}$ is constant and ≈ 2 as predicted by QCD, since the two reactions probe a different parton content of the proton. The ratio as a function of $E_T^{\rm jet}$ (Q^2) increases as $E_T^{\rm jet}$ (Q^2) increases, in good agreement with the prediction. The increase at high values of $E_T^{\rm jet}$ and Q^2 is expected due to the increasing contribution from the valence-quark densities in the proton at high x and the fact that both reactions are sensitive to different quark flavors. The behavior observed in the ratio of the measured cross sections as a function of Q^2 is similar to the ratio of u and d parton densities. The same behavior is observed as a function of x.

Figure 9 shows the contributions to the theoretical uncertainty from the terms beyond NLO, the parton-shower model and that coming from the uncertainty in the PDFs separately for e^-p and e^+p collisions. Also shown are calculations using other PDF sets. For inclusive-jet $e^\pm p$ CC cross sections, the uncertainty coming from that on the PDFs is dominant. At high $E_T^{\rm jet}$, Q^2 and x, the uncertainty in the predicted cross sections for positron beams is larger than those for electron beams. This difference in the uncertainty due to the PDFs in the calculations for e^- and e^+ beams can be attributed to the different flavor content probed: in e^-p (e^+p) at high x the W^- (W^+) will couple predominantly to the u (d) valence quark in the proton; at present, the uncertainty in the d parton density is larger than that for the u quark. Furthermore, the comparison with the calculations using other PDF sets shows a wide spread in the predictions, especially for positron beams. Therefore, these measurements, in a phase-space region where the other theoretical uncertainties are well under control, have the potential to constrain the flavor content of the proton if used together with other data in global fits. A fast and accurate method to perform fits to extract the proton PDFs on data sets that included jet cross sections in NC DIS and photoproduction was recently developed by the ZEUS Collaboration [48]; the result was a sizable reduction of the uncertainty on the gluon density at medium and high x. Using the data presented here and extending such a method to jet cross sections in CC DIS may help to constrain the u and d valence quark distributions at high x.

The integrated unpolarized inclusive-jet cross sections, $\sigma_{\rm jets}$, are shown in Table 14. The measured cross sections are in good agreement with the predictions of NLO QCD, also shown in the table using different PDF sets.

7.3 Dijet cross sections

Unpolarized dijet differential cross sections were measured in the kinematic regime $Q^2 > 200$ GeV^2 and $y < 0.9$. The cross sections were determined for jets with $E_T^{\rm jet1} > 14$ GeV, $E_T^{\rm jet2} > 5$ GeV and $-1 < \eta^{\rm jet} < 2.5$. Figure 10 and Tables 6 to 11, 15 and 16 show the unpolarized dijet differential cross sections as functions of $\overline{\eta}^{\rm jet}$, $\overline{E}_T^{\rm jet}$, Q^2 and the dijet invariant mass, $M^{\rm jj}$, where $\overline{\eta}^{\rm jet} = (\eta^{\rm jet1} + \eta^{\rm jet2})/2$ and $\overline{E}_T^{\rm jet} = (E_T^{\rm jet1} + E_T^{\rm jet2})/2$ in CC $e^{\pm}p$ DIS. The measured $\overline{\eta}^{\rm jet}$ cross section has a maximum at $\overline{\eta}^{\rm jet} \sim 1.25$. The measured cross section as a function of $\overline{E}_T^{\rm jet}$ exhibits a fall-off of two orders of magnitude for $\overline{E}_T^{\rm jet} \gtrsim 20$ GeV. For $200 < Q^2 \lesssim 2000$ GeV^2, the distribution displays a weak dependence on Q^2. Values of $M^{\rm jj}$ above 100 GeV are accessible with the present statistics.

The NLO QCD predictions are compared to the data in Fig. 10. Figure 11 shows the relative difference to the predictions. The NLO predictions do not give an adequate description in shape and normalization of the measured differential cross sections over the entire phase space considered. In particular, for $M^{\rm jj}$, the data tend to be above the predictions for $M^{\rm jj} \gtrsim 70$ GeV. It was reported [49] that calculations of jet cross sections in NC DIS computed using the MEPJET program differ by $5 - 8\%$ from the results from other NLO programs. Comparisons of inclusive-jet calculations for NC DIS in the kinematic range of the measurements presented here performed using MEPJET and DISENT [50] showed an agreement better than 1%. However, similar comparisons for dijet cross sections showed relative differences above $\sim 5\%$. For CC DIS, it is not possible to quantify the degree of accuracy of the calculations of MEPJET since no alternative program exists. The NLO predictions give a reasonable description of the ratios of the cross sections for e^-p and e^+p interactions (see Fig. 11). New implementations of the theory are crucially needed to use the differential dijet cross sections presented here in global fits to extract the proton PDFs.

The integrated unpolarized dijet cross sections are shown in Table 14. The measured cross sections are larger than the predictions of NLO QCD.

7.4 Measurements of three-jet cross sections and observation of four-jet events

Differential three-jet cross sections were measured in the kinematic regime $Q^2 > 200$ GeV^2 and $y < 0.9$. The cross sections were determined for jets with $E_T^{\rm jet1} > 14$ GeV, $E_T^{\rm jet2} > 5$ GeV, $E_T^{\rm jet3} > 5$ GeV and $-1 < \eta^{\rm jet} < 2.5$. Three-jet cross sections in CC DIS were measured for the first time in $e^{\pm}p$ collisions.

Figure 12 shows a three-jet candidate event in the ZEUS detector: a clear three-jet topology and large transverse momentum are observed. The three-jet selected sample

also contains 9 e^-p and 2 e^+p candidates with a fourth jet of transverse energy above 5 GeV in the $\eta^{\rm jet}$ range considered. One of these candidates is displayed in Fig. 13: the fourth jet is clearly observed in the ZEUS detector.

Figure 14 and Tables 6 to 11, 15 and 16 show the unpolarized three-jet differential cross sections as functions of $\overline{\eta}^{\rm jet}$, $\overline{E}_T^{\rm jet}$, Q^2 and the three-jet invariant mass, $M^{\rm 3j}$, where $\overline{\eta}^{\rm jet} = (\eta^{\rm jet1} + \eta^{\rm jet2} + \eta^{\rm jet3})/3$ and $\overline{E}_T^{\rm jet} = (E_T^{\rm jet1} + E_T^{\rm jet2} + E_T^{\rm jet3})/3$ in CC $e^\pm p$ DIS. Values of $M^{\rm 3j}$ above 100 GeV are accessible with the present statistics.

The predictions of LO QCD are compared to the data in Fig. 14. The currently available QCD calculations are only lowest order and cannot predict the normalization of the data. Therefore, they were scaled by 1.92 and 1.42 for e^-p and e^+p collisions, respectively, so as to reproduce the measured integrated three-jet cross section. The scaled LO calculations give a good description of the shape of the data. Figure 15 shows the relative difference between the data and the scaled predictions. The lower part of Fig. 15 shows the ratio of the differential cross sections for the e^-p and e^+p samples.

The integrated unpolarized three-jet cross sections are shown in Table 14. The predictions of LO QCD are also shown in the table.

8 Summary

Measurements of polarized and unpolarized integrated and differential multi-jet cross sections in CC $e^\pm p$ DIS were made using 0.36 fb^{-1} of data collected with the ZEUS detector at HERA II. The measurements were made in the kinematic region defined by $Q^2 > 200$ GeV^2 and $y < 0.9$. Jets were identified in the laboratory frame using the k_T cluster algorithm in the longitudinally invariant inclusive mode.

Polarized inclusive-jet cross sections were measured integrated over the phase-space region considered and differentially as functions of $\eta^{\rm jet}$, $E_T^{\rm jet}$, Q^2 and x for jets with $E_T^{\rm jet} > 14$ GeV and $-1 < \eta^{\rm jet} < 2.5$. The measured cross sections are in good agreement with the SM predictions. The ratios of the differential cross sections for negative and positive longitudinally-polarized lepton beams are also well described by the predictions.

Unpolarized differential inclusive-jet cross sections were measured as functions of $\eta^{\rm jet}$, $E_T^{\rm jet}$, Q^2 and x. The ratio of the differential cross sections for e^-p and e^+p collisions as a function of $\eta^{\rm jet}$ is ≈ 2 in the $\eta^{\rm jet}$ range measured, as predicted by the theory. The ratio as a function of $E_T^{\rm jet}$ (Q^2) increases as $E_T^{\rm jet}$ (Q^2) increases, in agreement with the expected increased contribution from the valence-quark densities in the proton at high x and the fact that both reactions are sensitive to different quark flavors. Dijet differential cross sections were measured for jets with $E_T^{\rm jet1} > 14$ GeV, $E_T^{\rm jet2} > 5$ GeV and $-1 < \eta^{\rm jet} < 2.5$.

Next-to-leading-order QCD predictions computed using the program MEPJET were compared to the data. The NLO QCD predictions give a good description of the measured inclusive-jet cross sections. A detailed study of the theoretical uncertainties was performed: they are dominated by the contribution from the PDFs. Furthermore, the uncertainties due to the PDFs are larger for e^+p than for e^-p collisions. Therefore, these measurements, if used together with other data in global fits, have the potential to constrain the flavor content of the proton at high x.

The comparison of the predictions with the measured dijet differential cross sections shows a poor agreement in shape and normalization. Improved implementations of the theory are crucially needed to use these dijet measurements in a global fit to constrain the proton PDFs.

Three-jet differential cross sections were measured for the first time in $e^{\pm}p$ collisions for jets with $E_T^{\mathrm{jet1}} > 14$ GeV, $E_T^{\mathrm{jet2}} > 5$ GeV, $E_T^{\mathrm{jet3}} > 5$ GeV and $-1 < \eta^{\mathrm{jet}} < 2.5$. The leading-order QCD predictions give a good description of the shape of the data. The three-jet sample also contains eleven candidates with a fourth jet of $E_T^{\mathrm{jet}} > 5$ GeV in the η^{jet} range considered.

Acknowledgements

We are grateful to the DESY directorate for their strong support and encouragement. We thank the HERA machine group whose outstanding efforts resulted in a successful upgrade of the HERA accelerator which made this work possible. We also thank the HERA polarimeter group for providing the measurements of the lepton-beam polarization. The design, construction and installation of the ZEUS detector were made possible by the efforts of many people not listed as authors.

References

[1] CDHS Coll., H. Abramowicz et al., Z. Phys. C 25 (1984) 29;
CDHSW Coll., J.P. Berge et al., Z. Phys. C 49 (1991) 187;
CCFR Coll., E. Oltman et al., Z. Phys. C 53 (1992) 51;
BEBC Coll., G.T. Jones et al., Z. Phys. C 62 (1994) 575.

[2] H1 Coll., T. Ahmed et al., Phys. Lett. B 324 (1994) 241;
H1 Coll., S. Aid et al., Z. Phys. C 67 (1995) 565;
H1 Coll., S. Aid et al., Phys. Lett. B 379 (1996) 319;
ZEUS Coll., M. Derrick et al., Phys. Rev. Lett. 75 (1995) 1006.

[3] ZEUS Coll., M. Derrick et al., Z. Phys. C 72 (1996) 47.

[4] ZEUS Coll., J. Breitweg et al., Eur. Phys. J. C 12 (2000) 411.

[5] H1 Coll., A. Aktas et al., Phys. Lett. B 634 (2006) 173.

[6] ZEUS Coll., S. Chekanov et al., Phys. Lett. B 637 (2006) 210.

[7] H1 Coll., C. Adloff et al., Eur. Phys. J. C 19 (2001) 429.

[8] ZEUS Coll., S. Chekanov et al., Eur. Phys. J. C 31 (2003) 149.

[9] ZEUS Coll., J. Breitweg et al., Eur. Phys. J. C 8 (1999) 367.

[10] ZEUS Coll., S. Chekanov et al., Phys. Lett. B 558 (2003) 41.

[11] ZEUS Coll., M. Derrick et al., Phys. Lett. B 293 (1992) 465.

[12] ZEUS Coll., U. Holm (ed.), *The ZEUS Detector*. Status Report (unpublished), DESY (1993), available on `http://www-zeus.desy.de/bluebook/bluebook.html`.

[13] N. Harnew et al., Nucl. Inst. Meth. A 279 (1989) 290;
B. Foster et al., Nucl. Phys. Proc. Suppl. B 32 (1993) 181;
B. Foster et al., Nucl. Inst. Meth. A 338 (1994) 254.

[14] A. Polini et al., Nucl. Inst. Meth. A 581 (2007) 656.

[15] P.D. Allfrey et al., Nucl. Inst. Meth. A 580 (2007) 1257.

[16] M. Derrick et al., Nucl. Inst. Meth. A 309 (1991) 77;
A. Andresen et al., Nucl. Inst. Meth. A 309 (1991) 101;
A. Caldwell et al., Nucl. Inst. Meth. A 321 (1992) 356;
A. Bernstein et al., Nucl. Inst. Meth. A 336 (1993) 23.

[17] J. Andruszków et al., Preprint DESY-92-066, DESY, 1992;
ZEUS Coll., M. Derrick et al., Z. Phys. C 63 (1994) 391;
J. Andruszków et al., Acta Phys. Pol. B 32 (2001) 2025.

[18] M. Helbich et al., Nucl. Inst. Meth. A 565 (2006) 572.

[19] A.A. Sokolov and I.M. Ternov, Sov. Phys. Dokl. 8 (1964) 1203.

[20] D.P. Barber et al., Nucl. Inst. Meth. A 329 (1993) 79.

[21] Polarization 2000 Group, V. Andreev et al., *A Proposal for an Upgrade of the HERA Polarimeters for HERA 2000*, Technical Report DESY PRC 98-07, DESY, 1998.

[22] M. Beckmann et al., Nucl. Inst. Meth. A 479 (2002) 334.

[23] F. Jacquet and A. Blondel, *Proc. of the Study for an ep Facility for Europe*, U. Amaldi (ed.), p. 391. Hamburg, Germany (1979). Also in preprint DESY 79/48.

[24] H. Wolfe, *Multi-jet cross sections in charged current $e^{\pm}p$ scattering at HERA*. Ph.D. Thesis, University of Wisconsin, Madison, 2008. (Unpublished).

[25] S. Catani et al., Nucl. Phys. B 406 (1993) 187.

[26] S.D. Ellis and D.E. Soper, Phys. Rev. D 48 (1993) 3160.

[27] J.E. Huth et al., *Research Directions for the Decade. Proc. of Summer Study on High Energy Physics, 1990*, E.L. Berger (ed.), p. 134. World Scientific (1992). Also in preprint FERMILAB-CONF-90-249-E.

[28] ZEUS Coll., S. Chekanov et al., Phys. Lett. B 547 (2002) 164.

[29] R. Brun et al., GEANT3, Technical Report CERN-DD/EE/84-1, CERN, 1987.

[30] G. Ingelman, A. Edin and J. Rathsman, Comp. Phys. Comm. 101 (1997) 108.

[31] A. Kwiatkowski, H. Spiesberger and H.-J. Möhring, Comp. Phys. Comm. 69 (1992) 155;
H. Spiesberger, *An Event Generator for ep Interactions at HERA Including Radiative Processes (Version 4.6)*, 1996, available on `http://www.desy.de/~hspiesb/heracles.html`.

[32] K. Charchuła, G.A. Schuler and H. Spiesberger, Comp. Phys. Comm. 81 (1994) 381;
H. Spiesberger, HERACLES *and* DJANGOH*: Event Generation for ep Interactions at HERA Including Radiative Processes*, 1998, available on `http://wwwthep.physik.uni-mainz.de/~hspiesb/djangoh/djangoh.html`.

[33] H.L. Lai et al., Eur. Phys. J. C 12 (2000) 375.

[34] Y. Azimov et al., Phys. Lett. B 165 (1985) 147;
G. Gustafson, Phys. Lett. B 175 (1986) 453;
G. Gustafson and U. Pettersson, Nucl. Phys. B 306 (1988) 746;
B. Andersson et al., Z. Phys. C 43 (1989) 625.

[35] L. Lönnblad, Comp. Phys. Comm. 71 (1992) 15;
L. Lönnblad, Z. Phys. C 65 (1995) 285.

[36] B. Andersson et al., Phys. Rep. 97 (1983) 31.

[37] T. Sjöstrand, Comp. Phys. Comm. 82 (1994) 74;
T. Sjöstrand et al., Comp. Phys. Comm. 135 (2001) 238.

[38] T. Sjöstrand, Comp. Phys. Comm. 39 (1986) 347;
T. Sjöstrand and M. Bengtsson, Comp. Phys. Comm. 43 (1987) 367.

[39] G. Marchesini et al., Comp. Phys. Comm. 67 (1992) 465;
G. Corcella et al., JHEP 0101 (2001) 010.

[40] E. Mirkes and D. Zeppenfeld, Phys. Lett. B 380 (1996) 205.

[41] W.T. Giele and E.W.N. Glover, Phys. Rev. D 46 (1992) 1980.

[42] ZEUS Coll., S. Chekanov et al., Phys. Rev. D 67 (2003) 012007.

[43] J. Pumplin et al., JHEP 0207 (2002) 012;
D. Stump et al., JHEP 0310 (2003) 046.

[44] A.D. Martin et al., Eur. Phys. J. C 28 (2003) 455.

[45] Particle Data Group, W.-M. Yao et al., J. Phys. G 33 (2006) 1.

[46] S. Bethke, Prog. Part. Nucl. Phys. 58 (2007) 351.

[47] M. Wing (on behalf of the ZEUS Coll.), *Proc. of the 10th International Conference on Calorimetry in High Energy Physics*, R. Zhu (ed.), p. 767. Pasadena, USA (2002). Also in preprint hep-ex/0206036.

[48] ZEUS Coll., S. Chekanov et al., Eur. Phys. J. C 42 (2005) 1.

[49] C. Duprel et al., Preprint hep-ph/9910448, 1999.

[50] S. Catani and M.H. Seymour, Nucl. Phys. B 485 (1997) 291. Erratum in Nucl. Phys. B 510 (1998) 503.

$\eta^{\rm jet}$ bin	$d\sigma/d\eta^{\rm jet}$ (pb)	$\delta_{\rm stat}$	$\delta_{\rm syst}$	$\delta_{\rm ES}$
$P_{e^-} = -0.27$ - inclusive jets				
$-1.0, -0.5$	4.22	± 0.38	± 0.32	$^{+0.17}_{-0.16}$
$-0.5, 0.0$	13.35	± 0.62	± 0.51	$^{+0.30}_{-0.29}$
$0.0, 0.5$	23.40	± 0.77	± 0.29	$^{+0.23}_{-0.22}$
$0.5, 1.0$	27.77	± 0.81	± 0.82	± 0.09
$1.0, 1.5$	28.30	± 0.82	± 0.92	$^{+0.08}_{-0.09}$
$1.5, 2.0$	24.71	± 0.79	± 0.40	$^{+0.10}_{-0.09}$
$2.0, 2.5$	19.41	± 0.87	± 2.36	± 0.15
$P_{e^-} = +0.30$ - inclusive jets				
$-1.0, -0.5$	2.81	± 0.37	± 0.21	$^{+0.11}_{-0.10}$
$-0.5, 0.0$	7.22	± 0.55	± 0.28	± 0.16
$0.0, 0.5$	12.45	± 0.67	± 0.47	$^{+0.12}_{-0.11}$
$0.5, 1.0$	16.05	± 0.74	± 0.48	± 0.05
$1.0, 1.5$	15.99	± 0.74	± 0.50	± 0.05
$1.5, 2.0$	15.34	± 0.75	± 0.42	$^{+0.06}_{-0.05}$
$2.0, 2.5$	11.39	± 0.80	± 1.37	± 0.09
$P_{e^+} = -0.37$ - inclusive jets				
$-1.0, -0.5$	1.26	± 0.28	± 0.14	± 0.04
$-0.5, 0.0$	3.33	± 0.38	± 0.16	± 0.05
$0.0, 0.5$	5.68	± 0.47	± 0.14	± 0.04
$0.5, 1.0$	6.64	± 0.49	± 0.40	± 0.04
$1.0, 1.5$	6.74	± 0.49	± 0.24	± 0.03
$1.5, 2.0$	6.52	± 0.50	± 0.07	± 0.04
$2.0, 2.5$	5.09	± 0.55	± 0.93	± 0.06
$P_{e^+} = +0.32$ - inclusive jets				
$-1.0, -0.5$	2.92	± 0.36	± 0.30	± 0.09
$-0.5, 0.0$	7.37	± 0.49	± 0.29	± 0.11
$0.0, 0.5$	10.34	± 0.54	± 0.41	± 0.08
$0.5, 1.0$	14.75	± 0.63	± 0.65	± 0.08
$1.0, 1.5$	12.38	± 0.58	± 0.65	± 0.06
$1.5, 2.0$	11.64	± 0.58	± 0.50	$^{+0.07}_{-0.06}$
$2.0, 2.5$	10.22	± 0.68	± 1.26	± 0.12

Table 1: *Differential polarized inclusive-jet cross-sections $d\sigma/d\eta^{\rm jet}$ for jets of hadrons in the laboratory frame selected with the longitudinally invariant k_T cluster algorithm. The statistical, uncorrelated systematic and energy-scale (*ES*) uncertainties are shown separately.*

$E_T^{\rm jet}$ bin (GeV)	$d\sigma/dE_T^{\rm jet}$ (pb/GeV)	$\delta_{\rm stat}$	$\delta_{\rm syst}$	$\delta_{\rm ES}$
$P_{e^-} = -0.27$ - inclusive jets				
14, 21	2.318	± 0.076	± 0.140	$^{+0.045}_{-0.051}$
21, 29	1.776	± 0.056	± 0.079	$^{+0.019}_{-0.018}$
29, 41	1.419	± 0.038	± 0.070	$^{+0.009}_{-0.010}$
41, 55	0.834	± 0.027	± 0.051	$^{+0.011}_{-0.010}$
55, 71	0.450	± 0.018	± 0.022	± 0.011
71, 87	0.212	± 0.012	± 0.057	$^{+0.003}_{-0.002}$
87, 120	0.0421	± 0.0035	± 0.0225	$^{+0.0063}_{-0.0050}$
$P_{e^-} = +0.30$ - inclusive jets				
14, 21	1.284	± 0.068	± 0.089	$^{+0.025}_{-0.028}$
21, 29	1.081	± 0.052	± 0.049	$^{+0.012}_{-0.011}$
29, 41	0.795	± 0.035	± 0.041	$^{+0.005}_{-0.006}$
41, 55	0.486	± 0.024	± 0.030	± 0.006
55, 71	0.263	± 0.017	± 0.016	$^{+0.007}_{-0.006}$
71, 87	0.106	± 0.010	± 0.029	± 0.001
87, 120	0.0276	± 0.0035	± 0.0149	$^{+0.0041}_{-0.0033}$
$P_{e^+} = -0.37$ - inclusive jets				
14, 21	0.761	± 0.053	± 0.058	± 0.012
21, 29	0.584	± 0.039	± 0.031	$^{+0.003}_{-0.004}$
29, 41	0.338	± 0.023	± 0.019	$^{+0.004}_{-0.003}$
41, 55	0.160	± 0.014	± 0.011	± 0.004
55, 71	0.0602	± 0.0079	± 0.0037	$^{+0.0025}_{-0.0023}$
71, 87	0.0157	± 0.0039	± 0.0047	$^{+0.0007}_{-0.0006}$
87, 120	0.00166	± 0.00083	± 0.00106	$^{+0.00032}_{-0.00025}$
$P_{e^+} = +0.32$ - inclusive jets				
14, 21	1.576	± 0.066	± 0.112	$^{+0.026}_{-0.024}$
21, 29	1.077	± 0.045	± 0.020	$^{+0.006}_{-0.007}$
29, 41	0.675	± 0.028	± 0.037	$^{+0.007}_{-0.006}$
41, 55	0.307	± 0.017	± 0.020	± 0.007
55, 71	0.1135	± 0.0094	± 0.0143	$^{+0.0047}_{-0.0043}$
71, 87	0.0374	± 0.0052	± 0.0083	$^{+0.0016}_{-0.0014}$
87, 120	0.0050	± 0.0012	± 0.0027	$^{+0.0010}_{-0.0008}$

Table 2: *Differential polarized inclusive-jet cross-sections $d\sigma/dE_T^{\rm jet}$. Other details as in the caption to Table 1.*

Q^2 bin (GeV^2)	$d\sigma/dQ^2$ (pb/GeV^2)	$\delta_{\rm stat}$	$\delta_{\rm syst}$	$\delta_{\rm ES}$
$P_{e^-} = -0.27$ - inclusive jets				
$200, 500$	0.0246	± 0.0013	± 0.0015	$^{+0.0024}_{-0.0023}$
$500, 1000$	0.02226	± 0.00079	± 0.00090	$^{+0.00061}_{-0.00059}$
$1000, 2000$	0.01578	± 0.00046	± 0.00053	± 0.00022
$2000, 4000$	0.00797	± 0.00023	± 0.00007	± 0.00004
$4000, 10000$	0.002532	± 0.000072	± 0.000134	± 0.000038
$10000, 20000$	0.000429	± 0.000022	± 0.000029	± 0.000018
$20000, 88000$	$1.4 \cdot 10^{-5}$	$\pm 1.3 \cdot 10^{-6}$	$\pm 5.7 \cdot 10^{-6}$	$\pm 1.4 \cdot 10^{-6}$
$P_{e^-} = +0.30$ - inclusive jets				
$200, 500$	0.0135	± 0.0011	± 0.0011	± 0.0013
$500, 1000$	0.01332	± 0.00074	± 0.00051	$^{+0.00036}_{-0.00035}$
$1000, 2000$	0.00926	± 0.00042	± 0.00030	± 0.00013
$2000, 4000$	0.00437	± 0.00020	± 0.00004	± 0.00002
$4000, 10000$	0.001364	± 0.000064	± 0.000075	± 0.000020
$10000, 20000$	$30.6 \cdot 10^{-5}$	$\pm 2.2 \cdot 10^{-5}$	$\pm 2.0 \cdot 10^{-5}$	$\pm 1.3 \cdot 10^{-5}$
$20000, 88000$	$8.1 \cdot 10^{-6}$	$\pm 1.2 \cdot 10^{-6}$	$\pm 3.3 \cdot 10^{-6}$	$\pm 0.8 \cdot 10^{-6}$
$P_{e^+} = -0.37$ - inclusive jets				
$200, 500$	0.00984	± 0.00096	± 0.00049	$^{+0.00091}_{-0.00087}$
$500, 1000$	0.00814	± 0.00058	± 0.00026	± 0.00016
$1000, 2000$	0.00463	± 0.00030	± 0.00022	± 0.00002
$2000, 4000$	0.00182	± 0.00013	± 0.00007	± 0.00003
$4000, 10000$	$34.1 \cdot 10^{-5}$	$\pm 3.1 \cdot 10^{-5}$	$\pm 2.0 \cdot 10^{-5}$	$\pm 1.4 \cdot 10^{-5}$
$10000, 20000$	$25.0 \cdot 10^{-6}$	$\pm 5.9 \cdot 10^{-6}$	$\pm 5.7 \cdot 10^{-6}$	$\pm 2.3 \cdot 10^{-6}$
$P_{e^+} = +0.32$ - inclusive jets				
$200, 500$	0.0198	± 0.0012	± 0.0010	$^{+0.0018}_{-0.0017}$
$500, 1000$	0.01586	± 0.00070	± 0.00023	$^{+0.00030}_{-0.00031}$
$1000, 2000$	0.00905	± 0.00036	± 0.00027	$^{+0.00004}_{-0.00004}$
$2000, 4000$	0.00345	± 0.00016	± 0.00014	$^{+0.00005}_{-0.00005}$
$4000, 10000$	$68.8 \cdot 10^{-5}$	$\pm 3.9 \cdot 10^{-5}$	$\pm 5.6 \cdot 10^{-5}$	$\pm 2.7 \cdot 10^{-5}$
$10000, 20000$	$61.3 \cdot 10^{-6}$	$\pm 8.0 \cdot 10^{-6}$	$\pm 10.0 \cdot 10^{-6}$	$\pm 5.6 \cdot 10^{-6}$
$20000, 88000$	$3.5 \cdot 10^{-7}$	$\pm 1.8 \cdot 10^{-7}$	$\pm 2.8 \cdot 10^{-7}$	$\pm 0.6 \cdot 10^{-7}$

Table 3: *Differential polarized inclusive-jet cross-sections $d\sigma/dQ^2$. Other details as in the caption to Table 1.*

x bin	$d\sigma/dx$ (pb/GeV)	$\delta_{\rm stat}$	$\delta_{\rm syst}$	$\delta_{\rm ES}$
$P_{e^-} = -0.27$ - inclusive jets				
$0.006, 0.025$	16.17	± 0.70	± 0.83	$^{+1.06}_{-1.01}$
$0.025, 0.063$	46.9	± 1.3	± 1.6	± 0.9
$0.063, 0.16$	60.6	± 1.4	± 0.9	± 0.2
$0.16, 0.40$	39.7	± 1.1	± 1.7	± 0.7
$0.40, 1.0$	3.94	± 0.33	± 0.53	± 0.29
$P_{e^-} = +0.30$ - inclusive jets				
$0.006, 0.025$	9.71	± 0.65	± 0.76	$^{+0.64}_{-0.61}$
$0.025, 0.063$	24.3	± 1.1	± 0.9	± 0.5
$0.063, 0.16$	36.6	± 1.3	± 0.6	± 0.1
$0.16, 0.40$	23.2	± 1.0	± 1.2	± 0.4
$0.40, 1.0$	2.21	± 0.30	± 0.38	± 0.16
$P_{e^+} = -0.37$ - inclusive jets				
$0.006, 0.025$	6.10	± 0.54	± 0.28	$^{+0.35}_{-0.34}$
$0.025, 0.063$	13.59	± 0.81	± 0.53	± 0.15
$0.063, 0.16$	14.90	± 0.82	± 0.62	± 0.16
$0.16, 0.40$	5.22	± 0.47	± 0.30	± 0.13
$0.40, 1.0$	0.33	± 0.11	± 0.12	± 0.02
$P_{e^+} = +0.32$ - inclusive jets				
$0.006, 0.025$	12.34	± 0.67	± 0.56	$^{+0.71}_{-0.69}$
$0.025, 0.063$	28.1	± 1.0	± 1.0	± 0.3
$0.063, 0.16$	26.57	± 0.95	± 0.88	± 0.29
$0.16, 0.40$	11.55	± 0.60	± 0.65	± 0.28
$0.40, 1.0$	0.50	± 0.12	± 0.06	± 0.04

Table 4: *Differential polarized inclusive-jet cross-sections $d\sigma/dx$. Other details as in the caption to Table 1.*

lepton and polarization	σ_{jets} (pb)	δ_{stat} (pb)	δ_{syst} (pb)	δ_{ES} (pb)	SM prediction (pb)
$P_{e^-} = -0.27 \pm 0.01$	70.54	0.97	0.58	$^{+0.43}_{-0.40}$	69.17
$P_{e^-} = +0.29 \pm 0.01$	40.53	0.88	0.45	$^{+0.24}_{-0.23}$	38.67
$P_{e^+} = -0.37^{+0.01}_{-0.02}$	17.55	0.60	0.57	± 0.11	16.86
$P_{e^+} = +0.32 \pm 0.01$	34.51	0.72	1.05	$^{+0.23}_{-0.22}$	35.33

Table 5: *Integrated polarized inclusive-jet cross-sections σ_{jets} for jets of hadrons in the laboratory frame selected with the longitudinally invariant k_T cluster algorithm. The statistical, uncorrelated systematic and energy-scale (*ES*) uncertainties are shown separately. The uncertainty coming from the luminosity measurement is not shown. The predictions of the Standard Model as given by the* MEPJET *calculation are shown in the last column.*

$\eta^{\rm jet}$ bin	$d\sigma/d\eta^{\rm jet}$ (pb)	$\delta_{\rm stat}$	$\delta_{\rm syst}$	$\delta_{\rm ES}$	$C_{\rm QED}$	$C_{\rm had}$
unpolarized - inclusive jets						
$-1.0, -0.5$	3.58	± 0.28	± 0.30	$^{+0.15}_{-0.13}$	0.97	0.93
$-0.5, 0.0$	10.38	± 0.43	± 0.35	$^{+0.24}_{-0.22}$	0.97	0.98
$0.0, 0.5$	18.06	± 0.53	± 0.34	± 0.17	0.98	0.99
$0.5, 1.0$	22.17	± 0.57	± 0.75	± 0.07	0.97	1.00
$1.0, 1.5$	22.38	± 0.58	± 0.90	± 0.07	0.97	1.00
$1.5, 2.0$	20.33	± 0.57	± 0.31	$^{+0.08}_{-0.07}$	0.96	1.01
$2.0, 2.5$	15.59	± 0.61	± 1.85	± 0.12	0.96	1.01
$\overline{\eta}^{\rm jet}$ bin	$d\sigma/d\overline{\eta}^{\rm jet}$ (pb)	$\delta_{\rm stat}$	$\delta_{\rm syst}$	$\delta_{\rm ES}$	$C_{\rm QED}$	$C_{\rm had}$
unpolarized - dijets						
$-1.0, -0.5$	0.103	± 0.073	± 0.003	$^{+0.033}_{-0.032}$	0.80	0.60
$-0.5, 0.0$	1.48	± 0.26	± 0.52	± 0.09	0.96	0.81
$0.0, 0.5$	3.63	± 0.33	± 0.88	± 0.12	0.97	0.89
$0.5, 1.0$	5.68	± 0.37	± 0.43	$^{+0.14}_{-0.13}$	0.98	0.91
$1.0, 1.5$	6.43	± 0.34	± 0.07	$^{+0.12}_{-0.11}$	0.97	0.92
$1.5, 2.0$	3.77	± 0.24	± 0.14	± 0.07	0.95	0.92
$2.0, 2.5$	0.58	± 0.10	± 0.05	± 0.01	0.93	0.88
unpolarized - three jets						
$0.0, 0.5$	0.49	± 0.18	± 0.49	$^{+0.03}_{-0.05}$	0.95	0.75
$0.5, 1.0$	1.05	± 0.21	± 0.15	$^{+0.05}_{-0.06}$	0.93	0.78
$1.0, 1.5$	1.06	± 0.17	± 0.13	$^{+0.04}_{-0.03}$	0.99	0.80
$1.5, 2.5$	0.246	± 0.046	± 0.053	$^{+0.009}_{-0.007}$	0.99	0.80

Table 6: *Differential unpolarized inclusive-jet, dijet and three-jet cross-sections $d\sigma/d\eta^{\rm jet}$ and $d\sigma/d\overline{\eta}^{\rm jet}$ in e^-p collisions for jets of hadrons in the laboratory frame selected with the longitudinally invariant k_T cluster algorithm. The statistical, uncorrelated systematic and jet-energy-scale (*ES*) uncertainties are shown separately. The multiplicative corrections for QED radiative effects, $C_{\rm QED}$, and the corrections for hadronization effects, $C_{\rm had}$, to be applied to the parton-level NLO QCD calculations, are shown in the last two columns.*

$\eta^{\rm jet}$ bin	$d\sigma/d\eta^{\rm jet}$ (pb)	$\delta_{\rm stat}$	$\delta_{\rm syst}$	$\delta_{\rm ES}$	$C_{\rm QED}$	$C_{\rm had}$
unpolarized - inclusive jets						
$-1.0, -0.5$	2.12	± 0.24	± 0.21	$^{+0.07}_{-0.06}$	0.92	0.94
$-0.5, 0.0$	5.45	± 0.34	± 0.23	± 0.08	0.94	0.98
$0.0, 0.5$	8.34	± 0.39	± 0.22	± 0.06	0.95	0.99
$0.5, 1.0$	10.90	± 0.43	± 0.54	± 0.06	0.95	1.00
$1.0, 1.5$	9.95	± 0.42	± 0.42	± 0.05	0.95	1.00
$1.5, 2.0$	9.48	± 0.42	± 0.26	$^{+0.06}_{-0.05}$	0.94	1.01
$2.0, 2.5$	7.88	± 0.48	± 1.15	± 0.09	0.93	1.02
$\overline{\eta}^{\rm jet}$ bin	$d\sigma/d\overline{\eta}^{\rm jet}$ (pb)	$\delta_{\rm stat}$	$\delta_{\rm syst}$	$\delta_{\rm ES}$	$C_{\rm QED}$	$C_{\rm had}$
unpolarized - dijets						
$-0.5, 0.0$	0.92	± 0.23	± 0.33	$^{+0.07}_{-0.05}$	0.94	0.83
$0.0, 0.5$	1.75	± 0.28	± 0.42	$^{+0.06}_{-0.05}$	0.94	0.90
$0.5, 1.0$	3.01	± 0.32	± 0.24	$^{+0.07}_{-0.06}$	0.95	0.94
$1.0, 1.5$	3.52	± 0.28	± 0.06	$^{+0.07}_{-0.06}$	0.95	0.94
$1.5, 2.0$	1.95	± 0.20	± 0.11	± 0.04	0.94	0.94
$2.0, 2.5$	0.287	± 0.073	± 0.043	$^{+0.008}_{-0.005}$	0.93	0.91
unpolarized - three jets						
$0.0, 0.5$	0.079	± 0.079	± 0.079	$^{+0.006}_{-0.003}$	0.92	0.72
$0.5, 1.0$	0.68	± 0.23	± 0.09	$^{+0.04}_{-0.03}$	0.93	0.79
$1.0, 1.5$	0.254	± 0.086	± 0.033	$^{+0.011}_{-0.010}$	0.94	0.81
$1.5, 2.5$	0.087	± 0.029	± 0.019	± 0.003	0.91	0.83

Table 7: *Differential unpolarized inclusive-jet, dijet and three-jet cross-sections $d\sigma/d\eta^{\rm jet}$ and $d\sigma/\overline{\eta}^{\rm jet}$ in e^+p collisions. Other details as in the caption to Table 6.*

$E_T^{\rm jet}$ bin (GeV)	$d\sigma/dE_T^{\rm jet}$ (pb/GeV)	$\delta_{\rm stat}$	$\delta_{\rm syst}$	$\delta_{\rm ES}$	$C_{\rm QED}$	$C_{\rm had}$
unpolarized - inclusive jets						
$14, 21$	1.819	± 0.053	± 0.120	$^{+0.035}_{-0.040}$	1.03	0.99
$21, 29$	1.449	± 0.040	± 0.040	$^{+0.016}_{-0.014}$	1.01	1.00
$29, 41$	1.118	± 0.027	± 0.042	$^{+0.007}_{-0.008}$	0.97	1.00
$41, 55$	0.668	± 0.019	± 0.039	± 0.008	0.95	1.00
$55, 71$	0.361	± 0.013	± 0.031	± 0.009	0.92	0.99
$71, 87$	0.1596	± 0.0082	± 0.0360	$^{+0.0020}_{-0.0015}$	0.88	0.99
$87, 120$	0.0355	± 0.0026	± 0.0190	$^{+0.0053}_{-0.0042}$	0.83	0.98
$\overline{E}_T^{\rm jet}$ bin (GeV)	$d\sigma/d\overline{E}_T^{\rm jet}$ (pb/GeV)	$\delta_{\rm stat}$	$\delta_{\rm syst}$	$\delta_{\rm ES}$	$C_{\rm QED}$	$C_{\rm had}$
unpolarized - dijets						
$9.5, 14$	0.345	± 0.032	± 0.017	± 0.004	1.03	0.88
$14, 21$	0.502	± 0.028	± 0.077	$^{+0.007}_{-0.004}$	0.99	0.91
$21, 29$	0.375	± 0.021	± 0.030	± 0.010	0.94	0.92
$29, 41$	0.156	± 0.011	± 0.005	± 0.007	0.92	0.90
$41, 55$	0.0390	± 0.0049	± 0.0107	$^{+0.0037}_{-0.0026}$	0.88	0.90
$55, 71$	0.0070	± 0.0023	± 0.0007	$^{+0.0014}_{-0.0016}$	0.90	0.95
$71, 87$	0.0021	± 0.0021	± 0.0021	$^{+0.0014}_{-0.0000}$	1.00	0.94
unpolarized - three jets						
$8, 9.5$	0.0096	± 0.0096	± 0.0025	$^{+0.0016}_{-0.0017}$	1.02	0.72
$9.5, 14$	0.060	± 0.015	± 0.015	± 0.001	1.02	0.77
$14, 21$	0.099	± 0.015	± 0.003	± 0.004	0.96	0.79
$21, 29$	0.0481	± 0.0087	± 0.0036	$^{+0.0030}_{-0.0027}$	0.92	0.78
$29, 41$	0.0078	± 0.0029	± 0.0008	$^{+0.0007}_{-0.0006}$	0.86	0.85

Table 8: *Differential unpolarized inclusive-jet, dijet and three-jet cross-sections $d\sigma/dE_T^{\rm jet}$ and $d\sigma/d\overline{E}_T^{\rm jet}$ in $e^- p$ collisions. Other details as in the caption to Table 6.*

$E_T^{\rm jet}$ bin (GeV)	$d\sigma/dE_T^{\rm jet}$ (pb/GeV)	$\delta_{\rm stat}$	$\delta_{\rm syst}$	$\delta_{\rm ES}$	$C_{\rm QED}$	$C_{\rm had}$
unpolarized - inclusive jets						
$14, 21$	1.200	± 0.046	± 0.087	$^{+0.020}_{-0.019}$	0.99	1.00
$21, 29$	0.863	± 0.033	± 0.029	$^{+0.005}_{-0.006}$	0.96	1.00
$29, 41$	0.522	± 0.019	± 0.025	± 0.005	0.93	1.00
$41, 55$	0.242	± 0.012	± 0.016	± 0.006	0.91	0.99
$55, 71$	0.0901	± 0.0067	± 0.0078	$^{+0.0037}_{-0.0034}$	0.87	0.99
$71, 87$	0.0269	± 0.0035	± 0.0067	$^{+0.0011}_{-0.0010}$	0.84	0.98
$87, 120$	0.00329	± 0.00078	± 0.00179	$^{+0.00064}_{-0.00050}$	0.79	0.97
$\overline{E}_T^{\rm jet}$ bin (GeV)	$d\sigma/d\overline{E}_T^{\rm jet}$ (pb/GeV)	$\delta_{\rm stat}$	$\delta_{\rm syst}$	$\delta_{\rm ES}$	$C_{\rm QED}$	$C_{\rm had}$
unpolarized - dijets						
$9.5, 14$	0.288	± 0.033	± 0.017	$^{+0.001}_{-0.002}$	0.99	0.90
$14, 21$	0.330	± 0.026	± 0.052	± 0.004	0.95	0.93
$21, 29$	0.190	± 0.018	± 0.015	$^{+0.007}_{-0.006}$	0.93	0.93
$29, 41$	0.0433	± 0.0066	± 0.0023	$^{+0.0026}_{-0.0022}$	0.88	0.93
$41, 55$	0.0112	± 0.0032	± 0.0031	$^{+0.0014}_{-0.0010}$	0.90	0.95
unpolarized - three jets						
$8, 9.5$	0.019	± 0.019	± 0.005	± 0.002	0.82	0.73
$9.5, 14$	0.040	± 0.013	± 0.010	± 0.001	0.96	0.76
$14, 21$	0.043	± 0.012	± 0.002	± 0.002	0.93	0.80
$21, 29$	0.0034	± 0.0024	± 0.0003	$^{+0.0003}_{-0.0002}$	0.86	0.82
$29, 41$	0.0018	± 0.0018	± 0.0002	$^{+0.0003}_{-0.0002}$	0.88	0.86

Table 9: *Differential unpolarized inclusive-jet, dijet and three-jet cross-sections $d\sigma/dE_T^{\rm jet}$ and $d\sigma/d\overline{E}_T^{\rm jet}$ in e^+p collisions. Other details as in the caption to Table 6.*

Q^2 bin (GeV^2)	$d\sigma/dQ^2$ (pb/GeV^2)	$\delta_{\rm stat}$	$\delta_{\rm syst}$	$\delta_{\rm ES}$	$C_{\rm QED}$	$C_{\rm had}$
unpolarized - inclusive jets						
$200, 500$	0.01921	± 0.00087	± 0.00131	$^{+0.00190}_{-0.00180}$	0.98	0.97
$500, 1000$	0.01803	± 0.00056	± 0.00047	$^{+0.00049}_{-0.00048}$	0.99	1.00
$1000, 2000$	0.01268	± 0.00032	± 0.00017	± 0.00018	0.98	1.00
$2000, 4000$	0.00623	± 0.00016	± 0.00006	± 0.00003	0.97	1.00
$4000, 10000$	0.001963	± 0.000050	± 0.000097	± 0.000029	0.95	1.00
$10000, 20000$	0.000376	± 0.000016	± 0.000045	$^{+0.000015}_{-0.000016}$	0.94	1.00
$20000, 88000$	$1.121 \cdot 10^{-5}$	$\pm 0.091 \cdot 10^{-5}$	$\pm 0.706 \cdot 10^{-5}$	$^{+0.113}_{-0.114} \cdot 10^{-5}$	0.93	1.00
unpolarized - dijets						
$200, 500$	0.00409	± 0.00091	± 0.00112	$^{+0.00094}_{-0.00083}$	1.00	0.91
$500, 1000$	0.00323	± 0.00031	± 0.00037	$^{+0.00027}_{-0.00026}$	0.97	0.92
$1000, 2000$	0.00251	± 0.00016	± 0.00004	± 0.00009	0.97	0.91
$2000, 4000$	0.001170	± 0.000071	± 0.000112	$^{+0.000024}_{-0.000023}$	0.96	0.91
$4000, 10000$	0.000343	± 0.000021	± 0.000029	± 0.000011	0.95	0.89
$10000, 20000$	$69.8 \cdot 10^{-6}$	$\pm 6.9 \cdot 10^{-6}$	$\pm 23.9 \cdot 10^{-6}$	$\pm 4.1 \cdot 10^{-6}$	0.99	0.87
$20000, 88000$	$2.11 \cdot 10^{-6}$	$\pm 0.37 \cdot 10^{-6}$	$\pm 1.62 \cdot 10^{-6}$	$\pm 0.26 \cdot 10^{-5}$	0.96	0.86
unpolarized - three jets						
$500, 1000$	0.00034	± 0.00018	± 0.00015	$^{+0.00006}_{-0.00005}$	0.98	0.78
$1000, 2000$	0.000306	± 0.000073	± 0.000025	$^{+0.000027}_{-0.000026}$	0.96	0.78
$2000, 4000$	0.000193	± 0.000034	± 0.000024	$^{+0.000011}_{-0.000010}$	0.95	0.79
$4000, 10000$	$5.04 \cdot 10^{-5}$	$\pm 0.93 \cdot 10^{-5}$	$\pm 2.18 \cdot 10^{-5}$	$\pm 0.20 \cdot 10^{-5}$	0.95	0.79
$10000, 20000$	$1.04 \cdot 10^{-5}$	$\pm 0.25 \cdot 10^{-5}$	$\pm 0.70 \cdot 10^{-5}$	$^{+0.09}_{-0.08} \cdot 10^{-5}$	0.95	0.75
$20000, 88000$	$1.34 \cdot 10^{-7}$	$\pm 0.99 \cdot 10^{-7}$	$\pm 0.06 \cdot 10^{-7}$	$\pm 0.19 \cdot 10^{-7}$	0.92	0.77

Table 10: *Differential unpolarized inclusive-jet, dijet and three-jet cross-sections $d\sigma/dQ^2$ in $e^- p$ collisions. Other details as in the caption to Table 6.*

Q^2 bin (GeV^2)	$d\sigma/dQ^2$ (pb/GeV^2)	$\delta_{\rm stat}$	$\delta_{\rm syst}$	$\delta_{\rm ES}$	$C_{\rm QED}$	$C_{\rm had}$
unpolarized - inclusive jets						
$200, 500$	0.01525	± 0.00082	± 0.00074	$^{+0.00141}_{-0.00134}$	0.96	0.97
$500, 1000$	0.01241	± 0.00050	± 0.00018	± 0.00024	0.96	1.00
$1000, 2000$	0.00707	± 0.00026	± 0.00021	± 0.00003	0.95	1.00
$2000, 4000$	0.00273	± 0.00011	± 0.00010	± 0.00004	0.94	1.00
$4000, 10000$	0.000530	± 0.000027	± 0.000037	± 0.000021	0.91	1.00
$10000, 20000$	$4.35 \cdot 10^{-5}$	$\pm 0.53 \cdot 10^{-5}$	$\pm 0.71 \cdot 10^{-5}$	$\pm 0.40 \cdot 10^{-5}$	0.88	1.00
$20000, 88000$	$2.3 \cdot 10^{-7}$	$\pm 1.1 \cdot 10^{-7}$	$\pm 1.5 \cdot 10^{-7}$	$\pm 0.4 \cdot 10^{-7}$	0.81	1.00
unpolarized - dijets						
$200, 500$	0.00204	± 0.00072	± 0.00051	$^{+0.00042}_{-0.00037}$	0.98	0.92
$500, 1000$	0.00301	± 0.00033	± 0.00033	$^{+0.00025}_{-0.00024}$	0.96	0.93
$1000, 2000$	0.00152	± 0.00014	± 0.00003	$^{+0.00004}_{-0.00003}$	0.95	0.93
$2000, 4000$	0.000605	± 0.000058	± 0.000060	± 0.000016	0.94	0.92
$4000, 10000$	0.000106	± 0.000013	± 0.000011	± 0.000006	0.91	0.92
$10000, 20000$	$9.3 \cdot 10^{-6}$	$\pm 2.4 \cdot 10^{-6}$	$\pm 3.2 \cdot 10^{-5}$	$^{+1.1}_{-1.0} \cdot 10^{-6}$	0.92	0.92
$20000, 88000$	$7.4 \cdot 10^{-8}$	$\pm 7.4 \cdot 10^{-8}$	$\pm 5.8 \cdot 10^{-8}$	$\pm 1.1 \cdot 10^{-8}$	0.93	0.88
unpolarized - three jets						
$500, 1000$	0.00038	± 0.00020	± 0.00017	± 0.00006	0.97	0.78
$1000, 2000$	0.000156	± 0.000055	± 0.000013	$^{+0.000014}_{-0.000013}$	0.91	0.80
$2000, 4000$	0.000065	± 0.000021	± 0.000008	$^{+0.000003}_{-0.000002}$	0.91	0.80
$4000, 10000$	$9.2 \cdot 10^{-6}$	$\pm 4.4 \cdot 10^{-6}$	$\pm 4.1 \cdot 10^{-6}$	$\pm 0.7 \cdot 10^{-6}$	0.88	0.79
$10000, 20000$	$4.6 \cdot 10^{-7}$	$\pm 4.6 \cdot 10^{-7}$	$\pm 3.1 \cdot 10^{-7}$	$\pm 0.6 \cdot 10^{-7}$	1.00	0.82

Table 11: *Differential unpolarized inclusive-jet, dijet and three-jet cross-sections $d\sigma/dQ^2$ in e^+p collisions. Other details as in the caption to Table 6.*

x bin	$d\sigma/dx$ (pb)	$\delta_{\rm stat}$	$\delta_{\rm syst}$	$\delta_{\rm ES}$	$C_{\rm QED}$	$C_{\rm had}$
unpolarized - inclusive jets						
$0.006, 0.025$	13.12	± 0.50	± 0.74	$^{+0.86}_{-0.82}$	0.95	1.01
$0.025, 0.063$	35.82	± 0.85	± 1.13	$^{+0.70}_{-0.69}$	0.98	1.00
$0.063, 0.16$	49.26	± 0.98	± 0.09	± 0.14	0.97	0.99
$0.16, 0.40$	31.81	± 0.77	± 1.30	$^{+0.53}_{-0.54}$	0.97	0.99
$0.40, 1.0$	3.11	± 0.23	± 0.30	± 0.23	0.95	0.98

Table 12: *Differential unpolarized inclusive-jet cross-sections $d\sigma/dx$ in $e^- p$ collisions. Other details as in the caption to Table 6.*

x bin	$d\sigma/dx$ (pb)	$\delta_{\rm stat}$	$\delta_{\rm syst}$	$\delta_{\rm ES}$	$C_{\rm QED}$	$C_{\rm had}$
unpolarized - inclusive jets						
$0.006, 0.025$	9.49	± 0.47	± 0.41	$^{+0.54}_{-0.53}$	0.93	1.01
$0.025, 0.063$	21.40	± 0.71	± 0.76	± 0.24	0.96	1.00
$0.063, 0.16$	21.64	± 0.69	± 0.76	$^{+0.24}_{-0.23}$	0.95	0.99
$0.16, 0.40$	8.55	± 0.41	± 0.48	± 0.21	0.93	0.98
$0.40, 1.0$	0.439	± 0.090	± 0.084	± 0.032	0.91	0.98

Table 13: *Differential unpolarized inclusive-jet cross-sections $d\sigma/dx$ in $e^+ p$ collisions. Other details as in the caption to Table 6.*

lepton/ jet multiplicity	σ_{jets} (pb)	δ_{stat} (pb)	δ_{syst} (pb)	δ_{ES} (pb)	QCD predictions (pb)		
					ZEUS-S	CTEQ6	MRST
e^-/inclusive jet	56.18	0.68	0.53	$^{+0.34}_{-0.32}$	54.47 ± 0.75	54.05	54.56
e^+/inclusive jet	26.88	0.51	0.82	$^{+0.18}_{-0.17}$	26.77 ± 0.45	25.85	26.49
e^-/dijet	10.87	0.34	0.80	$^{+0.24}_{-0.23}$	9.14 ± 0.35	9.05	9.26
e^+/dijet	5.83	0.29	0.45	$^{+0.13}_{-0.12}$	4.57 ± 0.19	4.38	4.55
e^-/three jet	1.52	0.15	0.09	± 0.06	0.79 ± 0.22	0.79	0.82
e^+/three jet	0.563	0.110	0.037	$^{+0.025}_{-0.022}$	0.397 ± 0.118	0.386	0.409

Table 14: *Integrated unpolarized jet cross-sections σ_{jets} for jets of hadrons in the laboratory frame selected with the longitudinally invariant k_T cluster algorithm. The statistical, uncorrelated systematic and energy-scale (*ES*) uncertainties are shown separately. The predictions of QCD as given by the* Mepjet *calculations using the ZEUS-S PDFs are shown at NLO for the inclusive-jet and dijet cross sections and at LO for the three-jet cross sections, together with the total theoretical uncertainty. Also shown are the total cross sections predicted by QCD using the CTEQ6 or MRST PDF sets.*

M^{jj} bin (GeV)	$d\sigma/dM^{\mathrm{jj}}$ (pb/GeV)	δ_{stat}	δ_{syst}	δ_{ES}	C_{QED}	C_{had}
unpolarized - dijets						
$10, 15$	0.090	± 0.011	± 0.010	± 0.001	1.02	0.87
$15, 20$	0.207	± 0.018	± 0.011	± 0.002	0.99	0.88
$20, 30$	0.284	± 0.016	± 0.032	$^{+0.005}_{-0.004}$	0.97	0.89
$30, 45$	0.250	± 0.014	± 0.028	$^{+0.006}_{-0.007}$	0.96	0.90
$45, 65$	0.0960	± 0.0083	± 0.0191	$^{+0.0051}_{-0.0038}$	0.95	0.94
$65, 90$	0.0385	± 0.0060	± 0.0058	$^{+0.0023}_{-0.0032}$	0.94	0.96
$90, 120$	0.0132	± 0.0046	± 0.0035	$^{+0.0023}_{-0.0016}$	0.97	0.96
M^{3j} bin (GeV)	$d\sigma/dM^{\mathrm{3j}}$ (pb/GeV)	δ_{stat}	δ_{syst}	δ_{ES}	C_{QED}	C_{had}
unpolarized - three jets						
$20, 30$	0.0069	± 0.0024	± 0.0017	± 0.0001	0.99	0.83
$30, 45$	0.0253	± 0.0045	± 0.0009	$^{+0.0006}_{-0.0008}$	0.99	0.76
$45, 65$	0.0307	± 0.0049	± 0.0012	$^{+0.0012}_{-0.0011}$	0.97	0.77
$65, 90$	0.0150	± 0.0034	± 0.0054	$^{+0.0014}_{-0.0012}$	0.94	0.79
$90, 120$	0.0036	± 0.0022	± 0.0001	$^{+0.0004}_{-0.0003}$	0.94	0.85

Table 15: *Differential unpolarized dijet and three-jet cross-sections $d\sigma/dM^{\mathrm{jj}}$ and $d\sigma/dM^{\mathrm{3j}}$ in $e^- p$ collisions. Other details as in the caption to Table 6.*

$M^{\rm jj}$ bin (GeV)	$d\sigma/dM^{\rm jj}$ (pb/GeV)	$\delta_{\rm stat}$	$\delta_{\rm syst}$	$\delta_{\rm ES}$	$C_{\rm QED}$	$C_{\rm had}$
unpolarized - dijets						
$10, 15$	0.069	± 0.011	± 0.007	± 0.001	0.96	0.90
$15, 20$	0.146	± 0.017	± 0.010	$^{+0.001}_{-0.002}$	0.96	0.90
$20, 30$	0.171	± 0.015	± 0.022	± 0.003	0.95	0.91
$30, 45$	0.108	± 0.010	± 0.013	± 0.003	0.95	0.93
$45, 65$	0.0522	± 0.0077	± 0.0103	$^{+0.0023}_{-0.0025}$	0.94	0.95
$65, 90$	0.0169	± 0.0052	± 0.0026	$^{+0.0015}_{-0.0011}$	0.94	0.97
$90, 120$	0.0020	± 0.0020	± 0.0002	$^{+0.0003}_{-0.0002}$	0.92	0.99
$M^{\rm 3j}$ bin (GeV)	$d\sigma/dM^{\rm 3j}$ (pb/GeV)	$\delta_{\rm stat}$	$\delta_{\rm syst}$	$\delta_{\rm ES}$	$C_{\rm QED}$	$C_{\rm had}$
unpolarized - three jets						
$20, 30$	0.0051	± 0.0024	± 0.0013	± 0.0001	0.91	0.84
$30, 45$	0.0124	± 0.0037	± 0.0006	$^{+0.0005}_{-0.0003}$	0.95	0.75
$45, 65$	0.0076	± 0.0029	± 0.0007	± 0.0004	0.94	0.78
$65, 90$	0.0049	± 0.0024	± 0.0018	$^{+0.0005}_{-0.0004}$	0.90	0.81

Table 16: *Differential unpolarized dijet and three-jet cross-sections $d\sigma/dM^{\rm jj}$ and $d\sigma/dM^{\rm 3j}$ in e^+p collisions. Other details as in the caption to Table 6.*

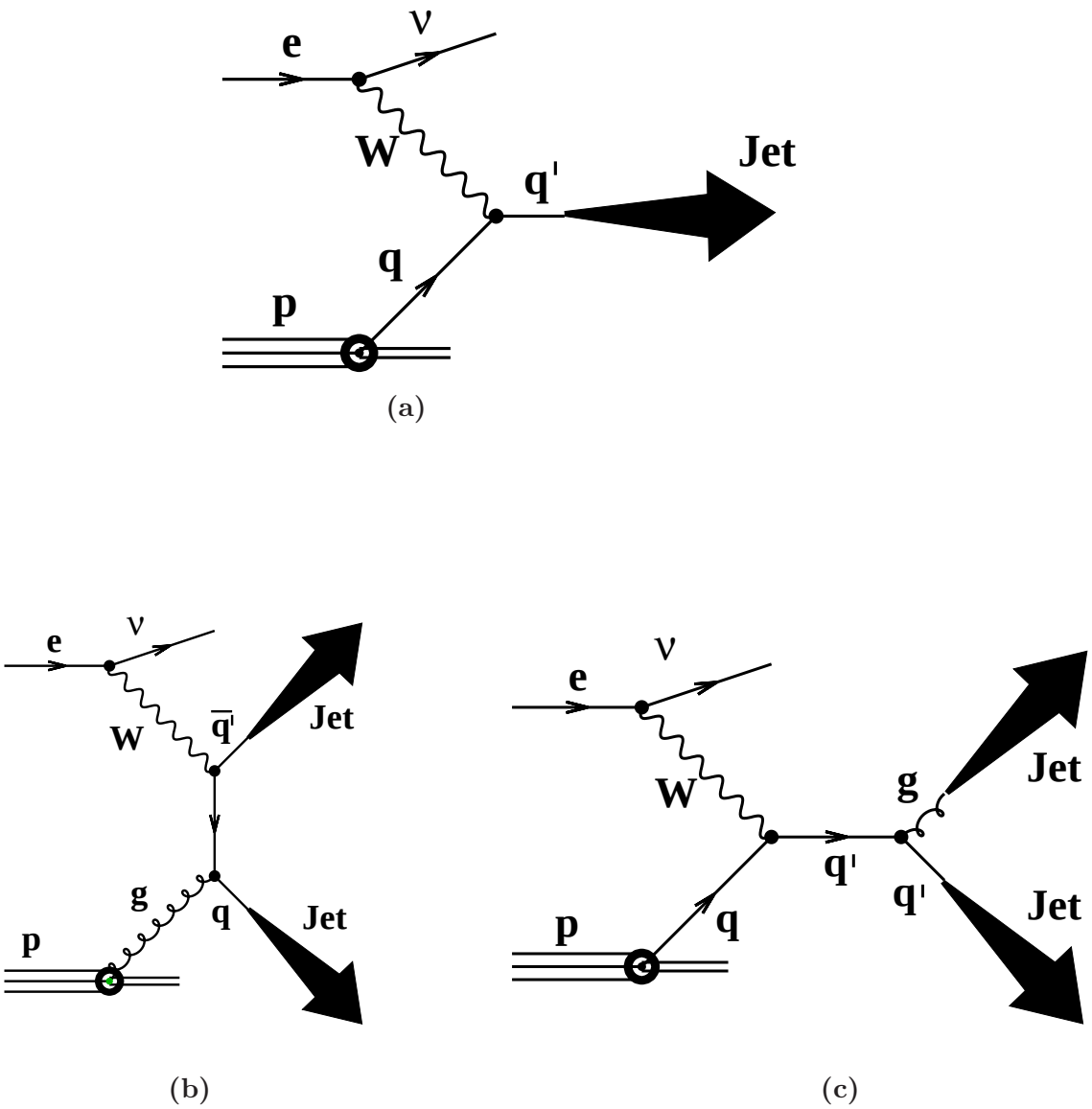

Figure 1: *Examples of jet production up to $\mathcal{O}(\alpha_s)$ in CC DIS. Feynman diagrams for: (a) quark-parton model, (b) boson-gluon fusion and (c) QCD-Compton processes.*

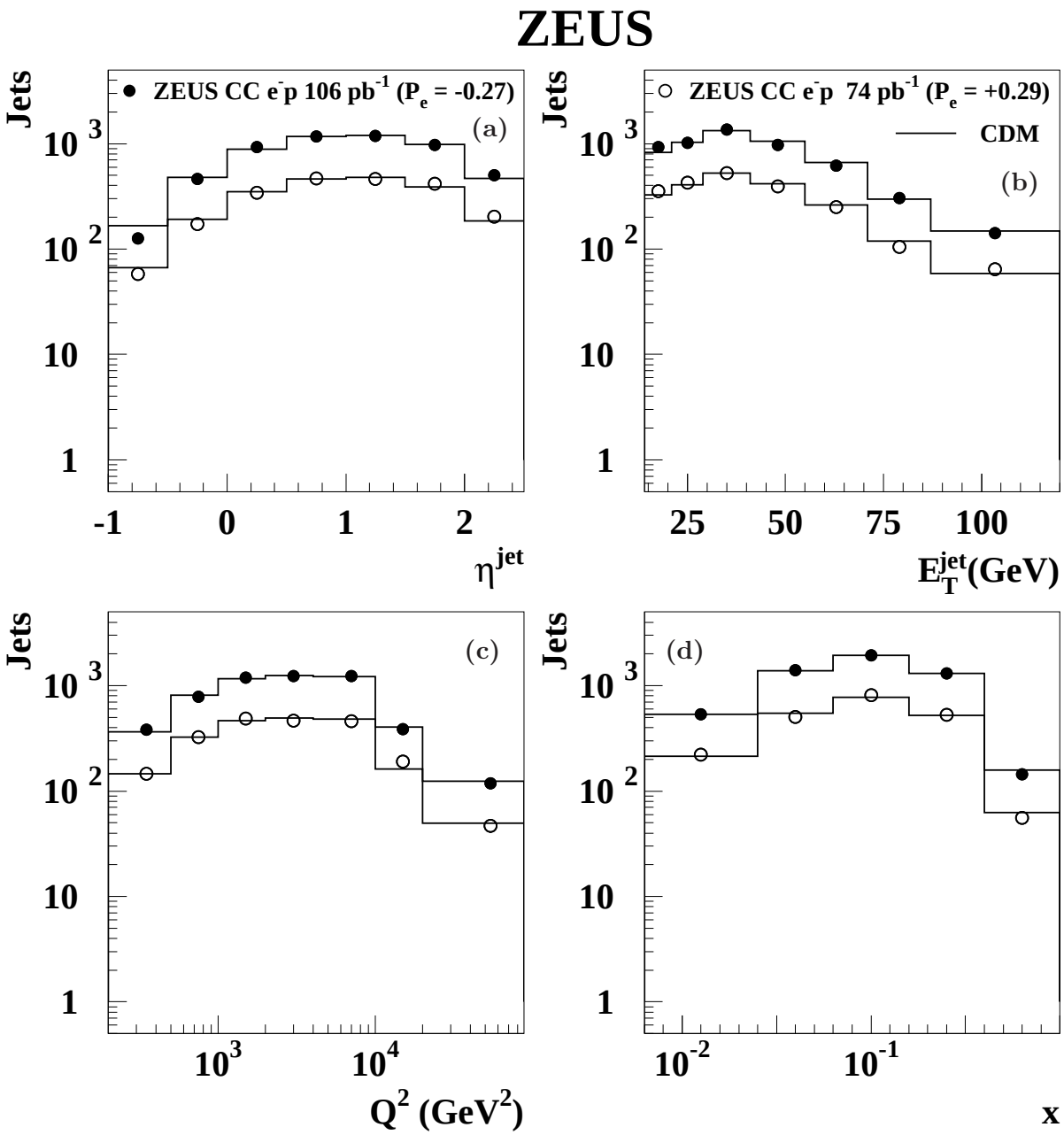

Figure 2: *Detector-level data distributions for inclusive-jet production with negative (dots) and positive (open circles) longitudinally polarized electron beams with* $E_T^{\rm jet} > 14$ *GeV and* $-1 < \eta^{\rm jet} < 2.5$ *in the kinematic region given by* $Q^2 > 200$ GeV^2 *and* $y < 0.9$ *as functions of (a)* $\eta^{\rm jet}$*, (b)* $E_T^{\rm jet}$*, (c)* Q^2 *and (d) Bjorken* x*. For comparison, the distributions of the CDM Monte Carlo model normalized to the number of jets in the data (solid histograms) are included.*

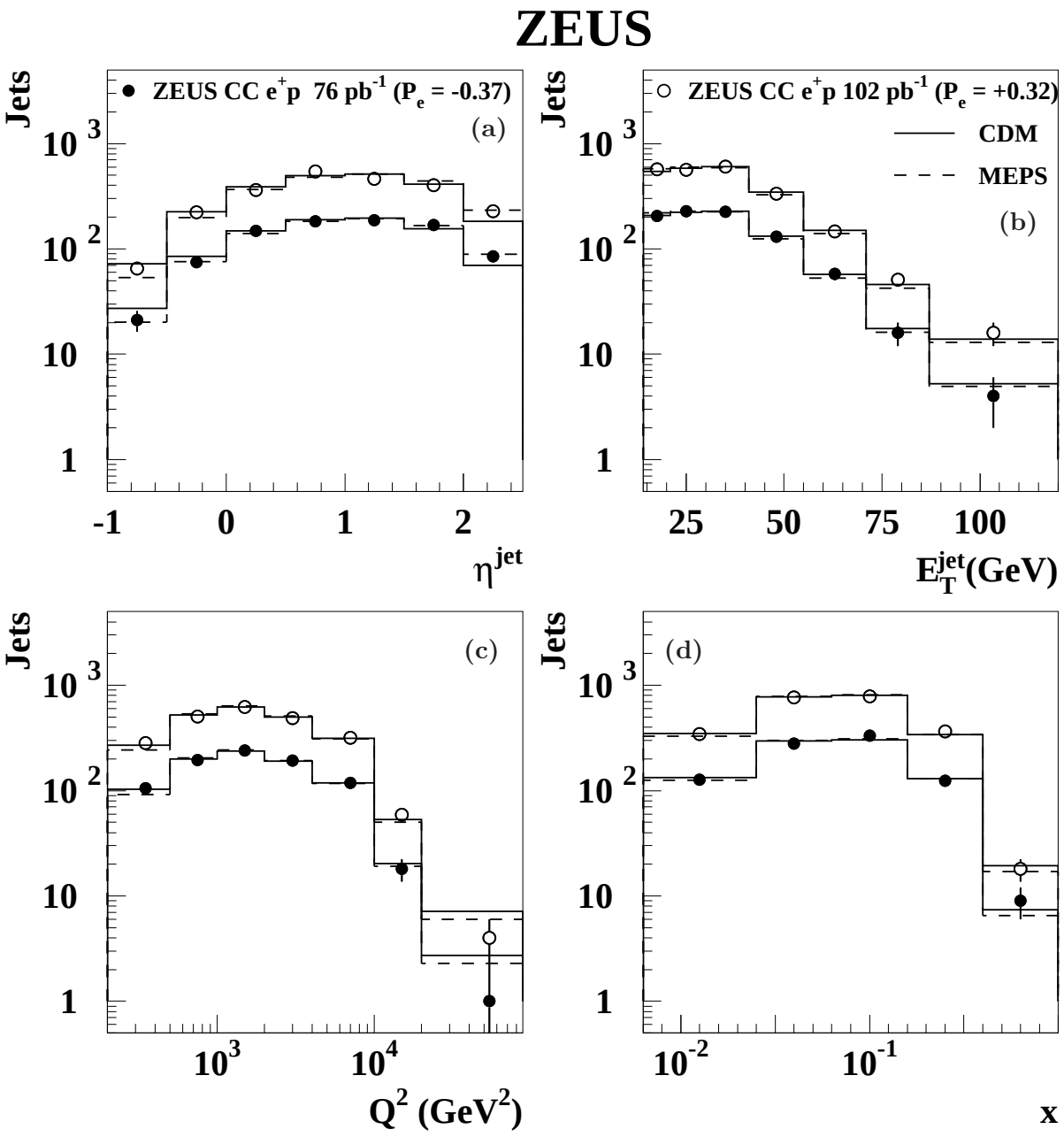

Figure 3: *Detector-level data distributions for inclusive-jet production with negative (dots) and positive (open circles) longitudinally polarized positron beams with* $E_T^{\rm jet} > 14$ *GeV and* $-1 < \eta^{\rm jet} < 2.5$ *in the kinematic region given by* $Q^2 > 200$ *GeV*^{2} *and* $y < 0.9$ *as functions of (a)* $\eta^{\rm jet}$*, (b)* $E_T^{\rm jet}$*, (c)* Q^2 *and (d) Bjorken* x*. The distributions of the* LEPTO-*MEPS Monte Carlo model are also included (dashed histograms). Other details as in the caption to Fig. 2.*

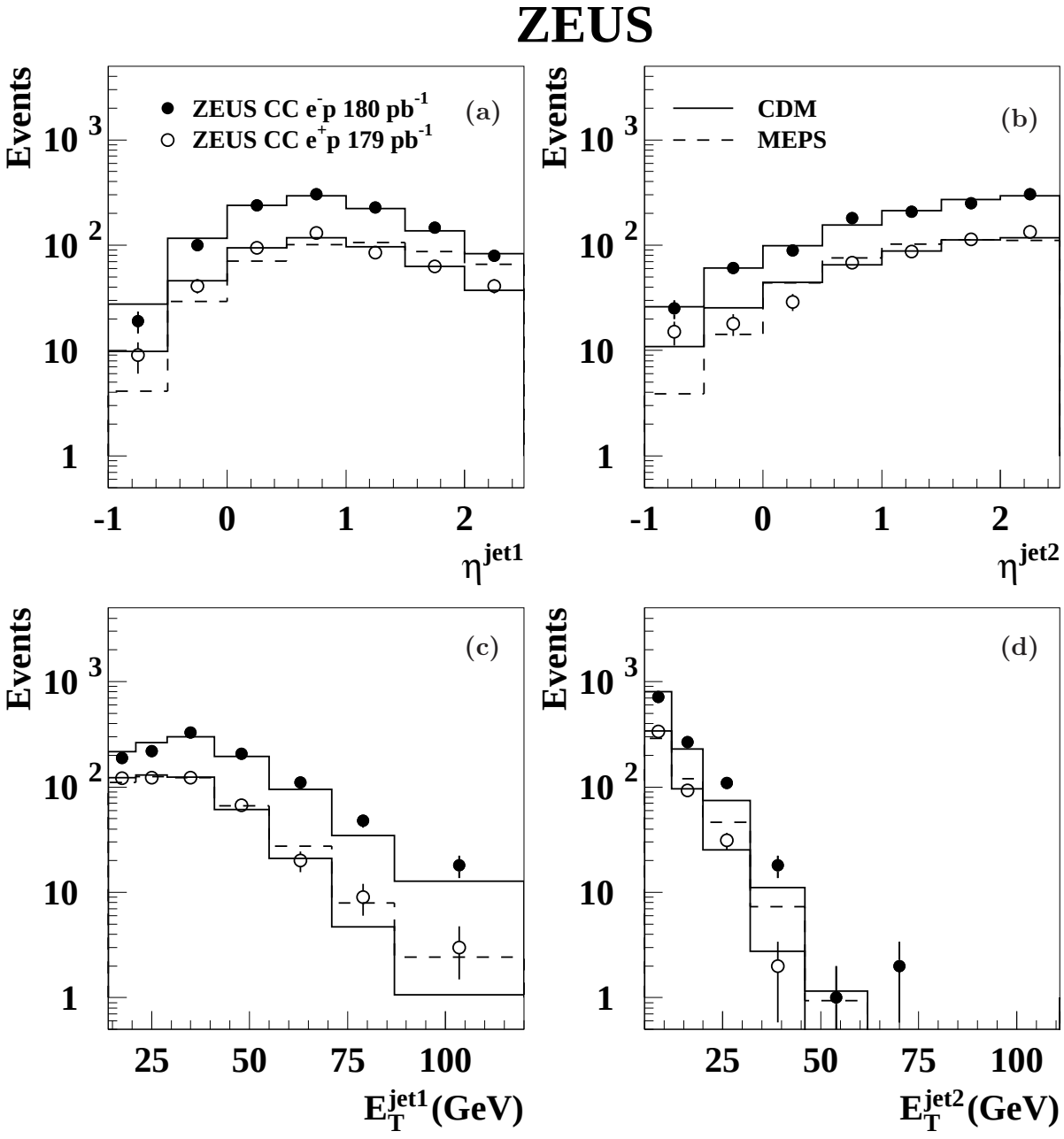

Figure 4: *Detector-level data distributions for dijet production with electron (dots) and positron (open circles) beams with* $E_T^{\rm jet1} > 14$ *GeV,* $E_T^{\rm jet2} > 5$ *GeV and* $-1 < \eta^{\rm jet} < 2.5$ *in the kinematic region given by* $Q^2 > 200$ *GeV*^{2} *and* $y < 0.9$ *as functions of (a)* $\eta^{\rm jet1}$*, (b)* $\eta^{\rm jet2}$*, (c)* $E_T^{\rm jet1}$ *and (d)* $E_T^{\rm jet2}$*. Other details as in the caption to Fig. 2.*

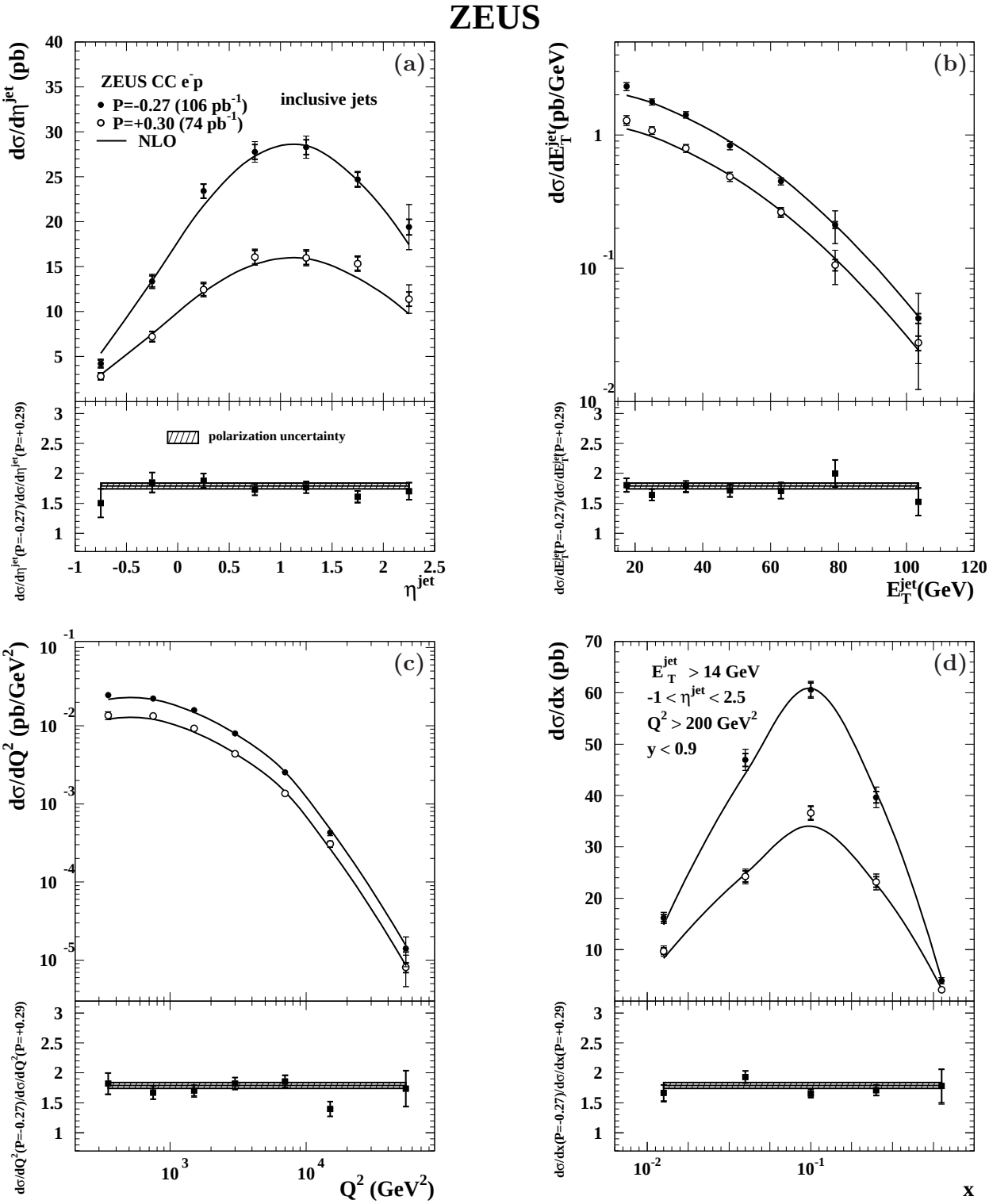

Figure 5: *Measured inclusive-jet cross sections in CC e^-p DIS for jets with $E_T^{\rm jet} > 14$ GeV and $-1 < \eta^{\rm jet} < 2.5$ in the kinematic regime given by $Q^2 > 200$ GeV^2 and $y < 0.9$ as functions of (a) $\eta^{\rm jet}$, (b) $E_T^{\rm jet}$, (c) Q^2 and (d) Bjorken x for negative (dots) and positive (open circles) longitudinally polarized electron beams. The data points are plotted at the bin centres. The inner error bars represent the statistical uncertainties of the data, and the outer error bars show the statistical and uncorrelated systematic uncertainties added in quadrature. For comparison, the predictions of NLO QCD (solid lines) are included. The lower parts of the figures display the ratio of the cross sections for negatively- and positively-polarized electron beams (squares) and the prediction (solid line) for the measured polarizations. The hatched band displays the uncertainty due to the polarization measurement.*

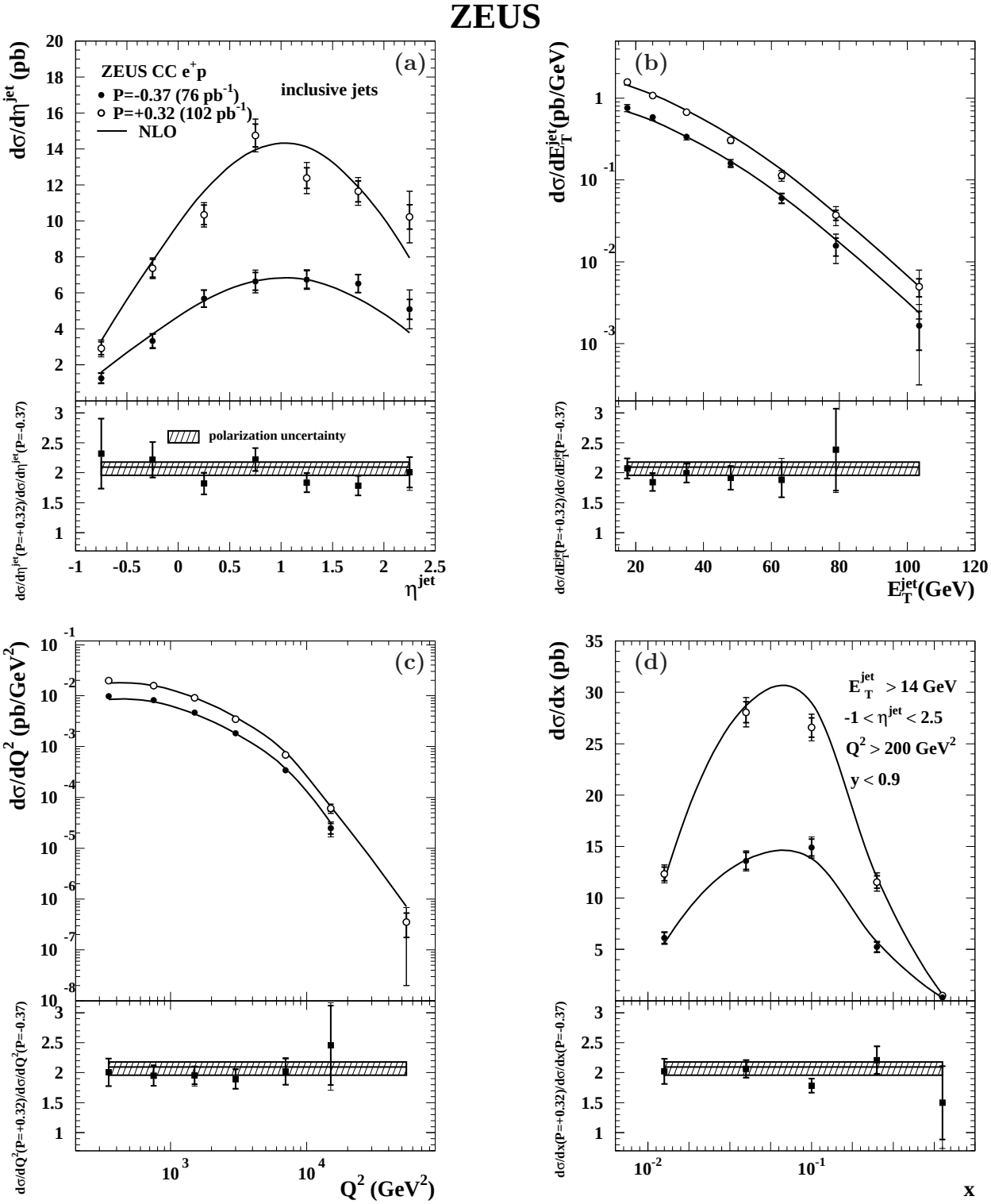

Figure 6: *Measured inclusive-jet cross sections in CC e^+p DIS for jets with $E_T^{\rm jet} > 14$ GeV and $-1 < \eta^{\rm jet} < 2.5$ in the kinematic regime given by $Q^2 > 200$ GeV^2 and $y < 0.9$ as functions of (a) $\eta^{\rm jet}$, (b) $E_T^{\rm jet}$, (c) Q^2 and (d) Bjorken x for negative (dots) and positive (open circles) longitudinally polarized electron beams. Other details as in the caption to Fig. 5.*

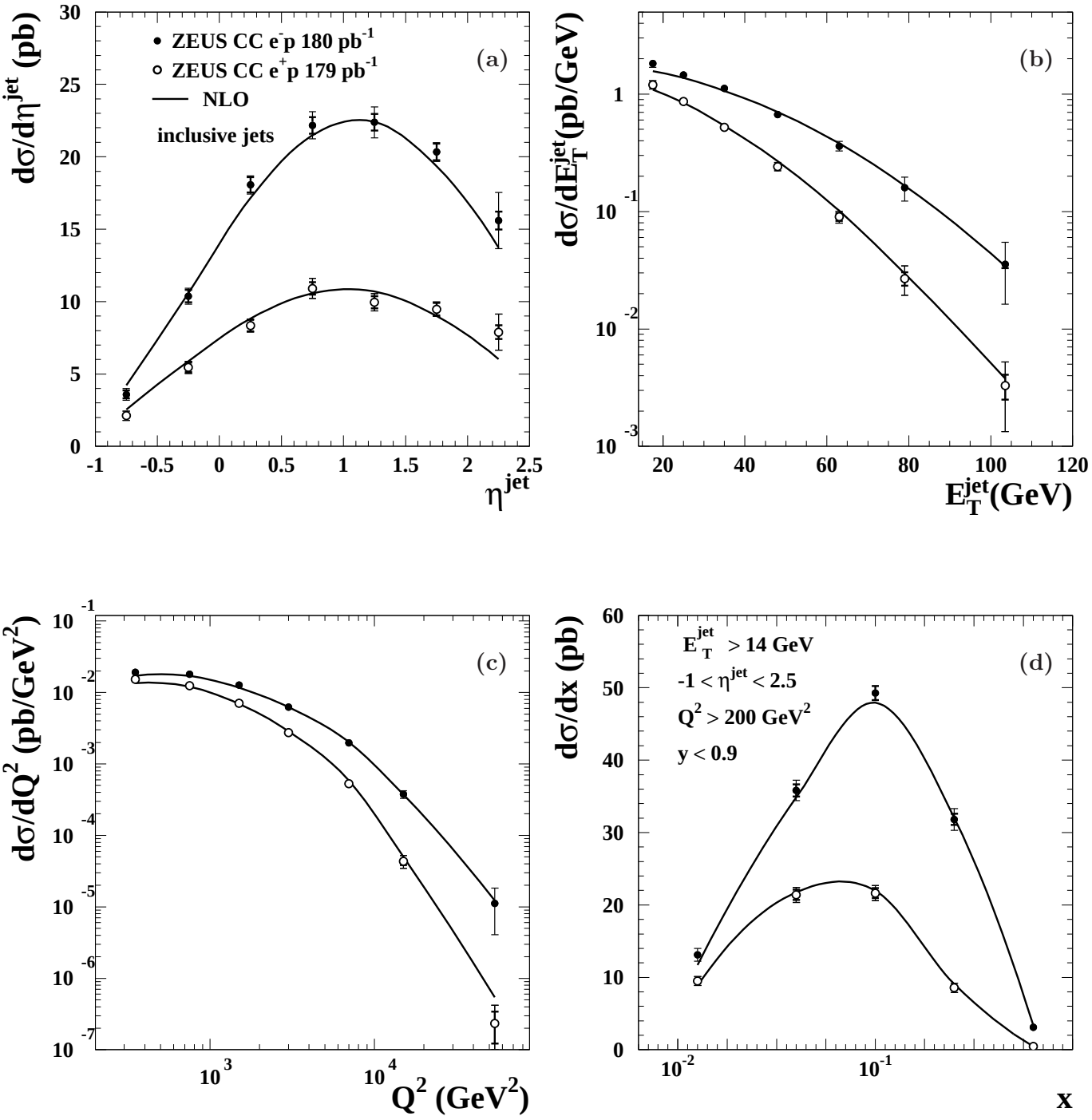

Figure 7: *Measured unpolarized inclusive-jet cross sections in CC DIS for jets with* $E_T^{\rm jet} > 14$ *GeV and* $-1 < \eta^{\rm jet} < 2.5$ *in the kinematic regime given by* $Q^2 > 200$ GeV^2 *and* $y < 0.9$ *as functions of (a)* $\eta^{\rm jet}$*, (b)* $E_T^{\rm jet}$*, (c)* Q^2 *and (d) Bjorken* x *in* e^-p *(dots) and* e^+p *(open circles) collisions. For comparison, the predictions of NLO QCD based on the* MEPJET *calculations using the ZEUS PDF sets (solid lines) are also shown. Other details as in the caption to Fig. 5.*

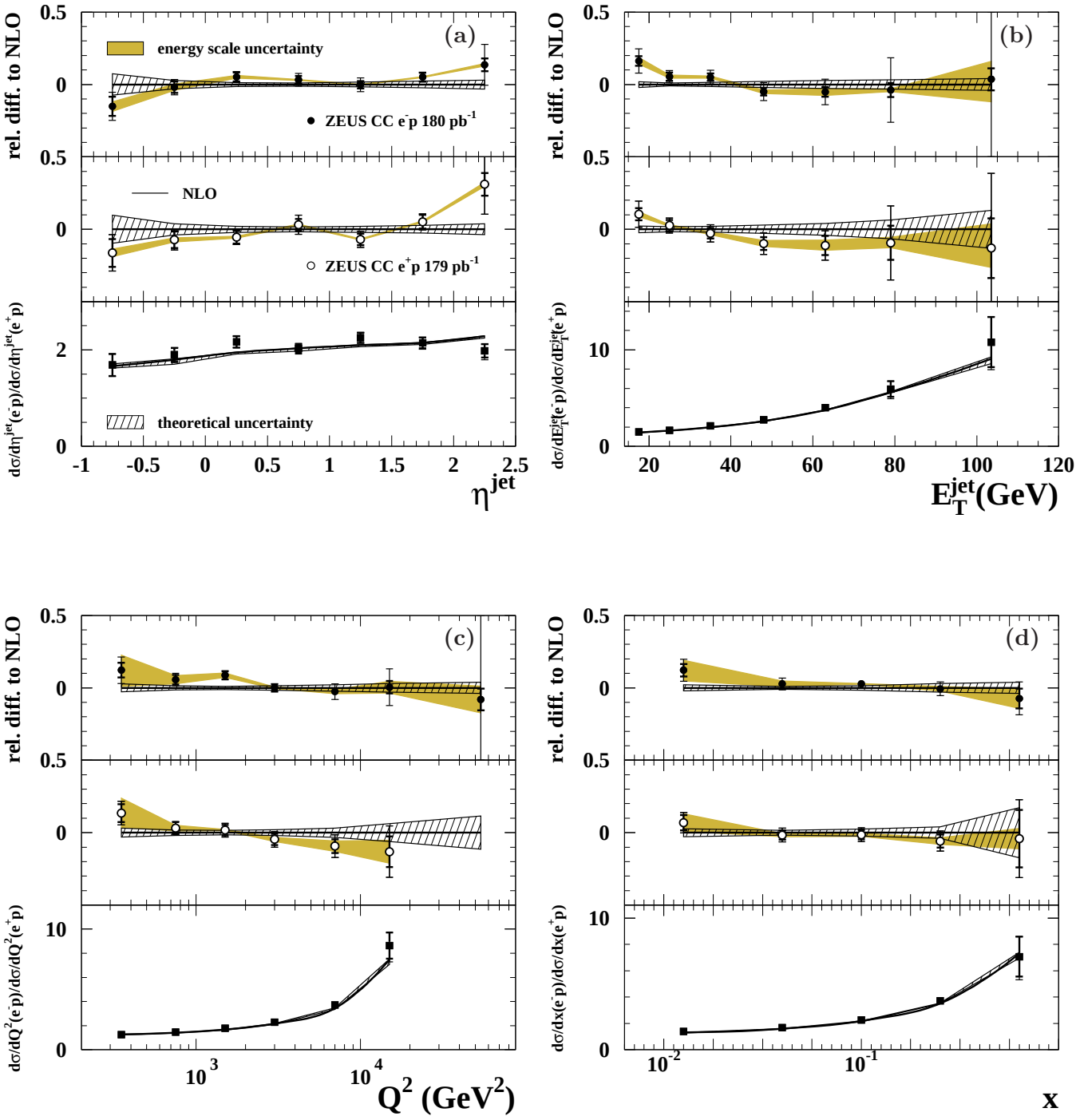

Figure 8: *Relative difference between the measured cross sections of Fig. 7 and the corresponding NLO QCD predictions in e^-p (dots) and e^+p (open circles) collisions as functions of (a) $\eta^{\rm jet}$, (b) $E_T^{\rm jet}$, (c) Q^2 and (d) Bjorken x. The lower parts of the figures display the ratio of the cross sections for e^-p and e^+p collisions (squares). The hatched areas display the theoretical uncertainty and the shaded areas display the uncertainty due to the absolute energy scale. Other details as in the caption to Fig. 5.*

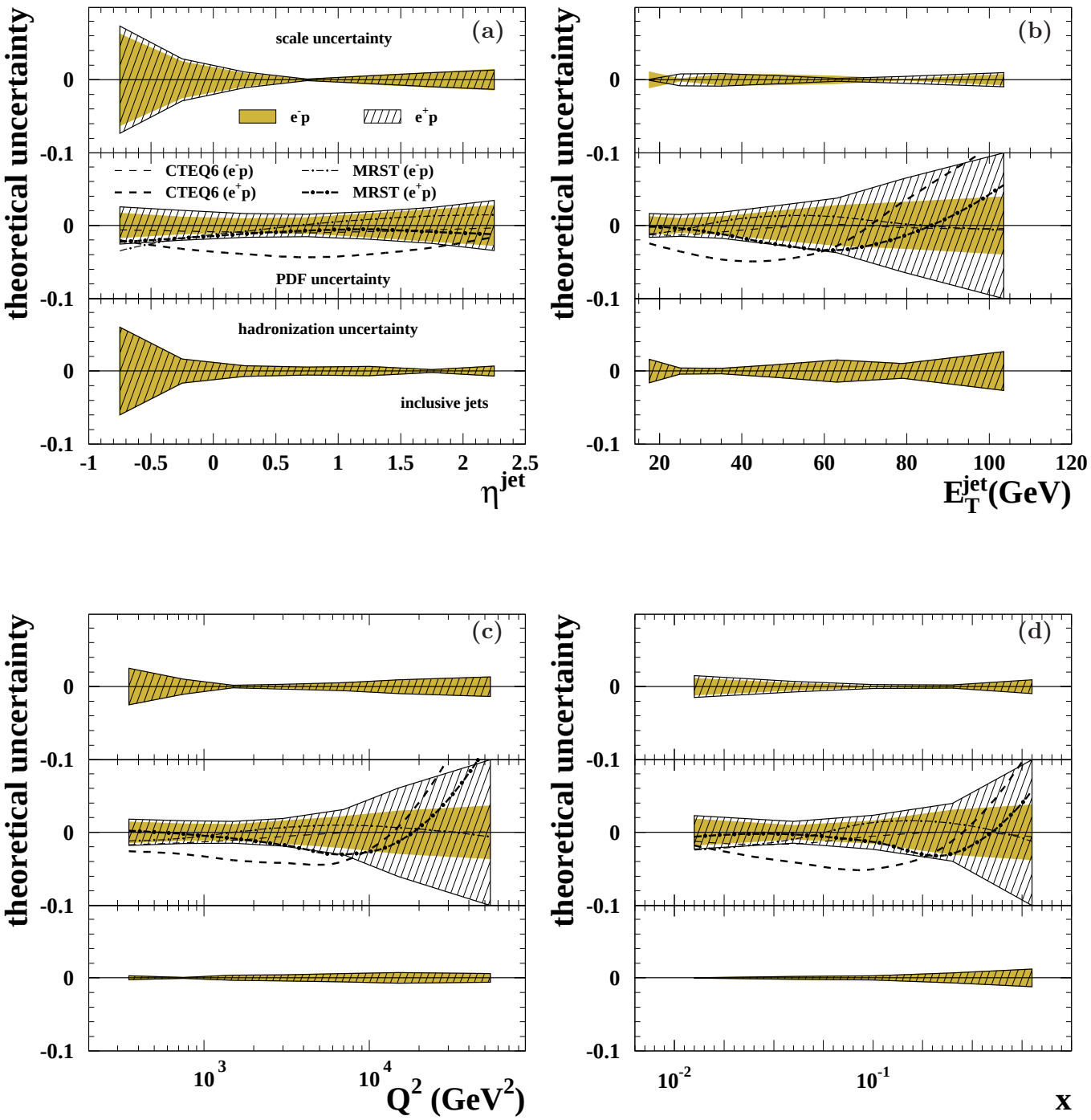

Figure 9: *Overview of theoretical uncertainties for the inclusive-jet cross sections in CC DIS for jets with $E_T^{\rm jet} > 14$ GeV and $-1 < \eta^{\rm jet} < 2.5$ in the kinematic regime given by $Q^2 > 200$ GeV^2 and $y < 0.9$ as functions of (a) $\eta^{\rm jet}$, (b) $E_T^{\rm jet}$, (c) Q^2 and (d) Bjorken x in e^-p (shaded areas) and e^+p (hatched areas) collisions. Shown are the relative uncertainties induced by the variation of the renormalization scale μ_R, the uncertainties on the proton PDFs and hadronisation model. Also shown are the relative differences between the NLO QCD calculations using the CTEQ6 (dashed lines) or MRST (dot-dashed lines) PDF sets to the calculations based on the ZEUS sets.*

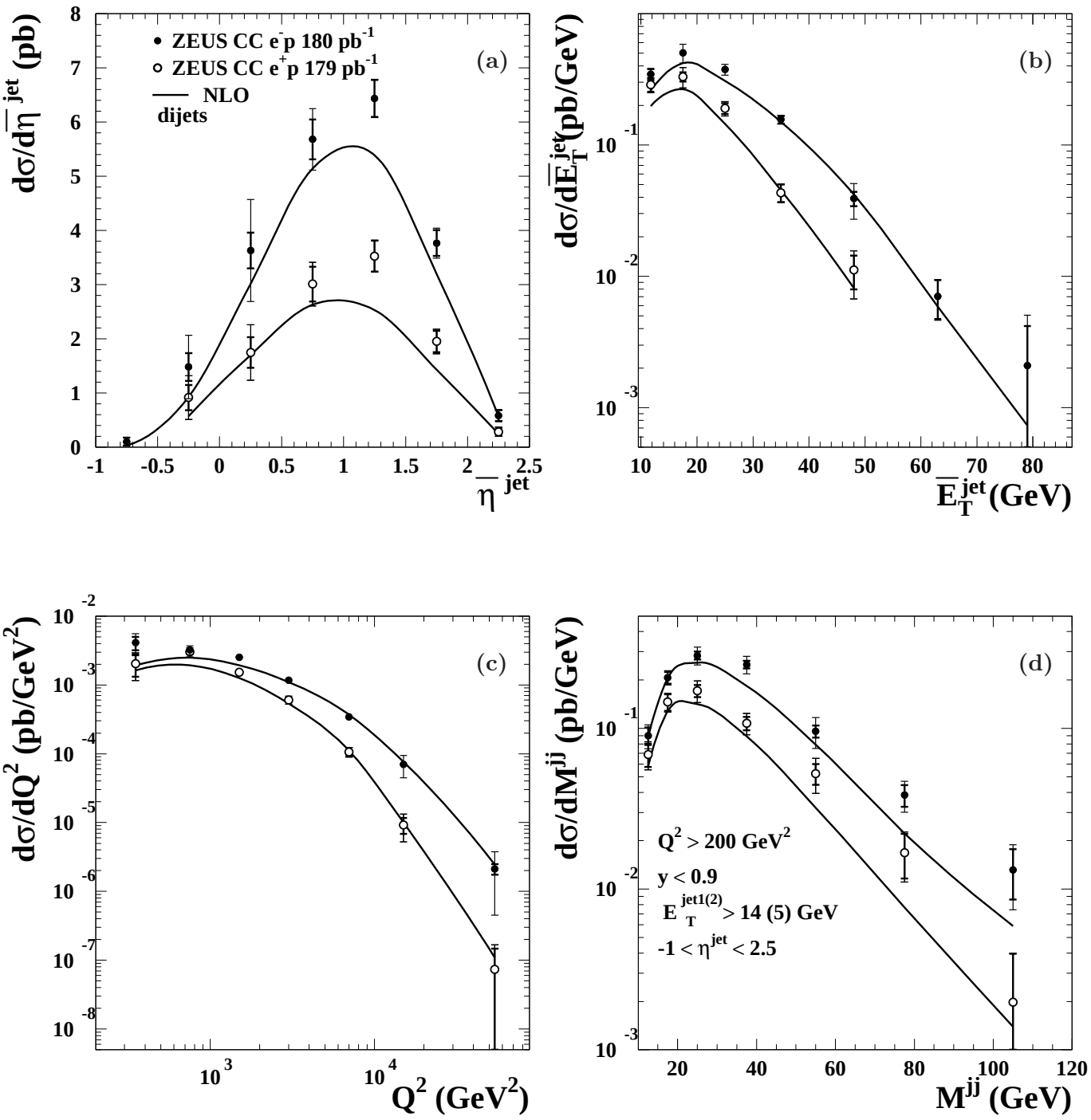

Figure 10: *Measured unpolarized dijet cross sections in CC DIS for jets with* $E_T^{\rm jet1} > 14$ *GeV,* $E_T^{\rm jet2} > 5$ *GeV and* $-1 < \eta^{\rm jet} < 2.5$ *in the kinematic regime given by* $Q^2 > 200$ *GeV*^{2} *and* $y < 0.9$ *as functions of (a)* $\overline{\eta}^{\rm jet}$*, (b)* $\overline{E}_T^{\rm jet}$*, (c)* Q^2 *and (d)* $M^{\rm jj}$ *in* e^-p *(dots) and* e^+p *(open circles) collisions. Other details as in the caption to Fig. 7.*

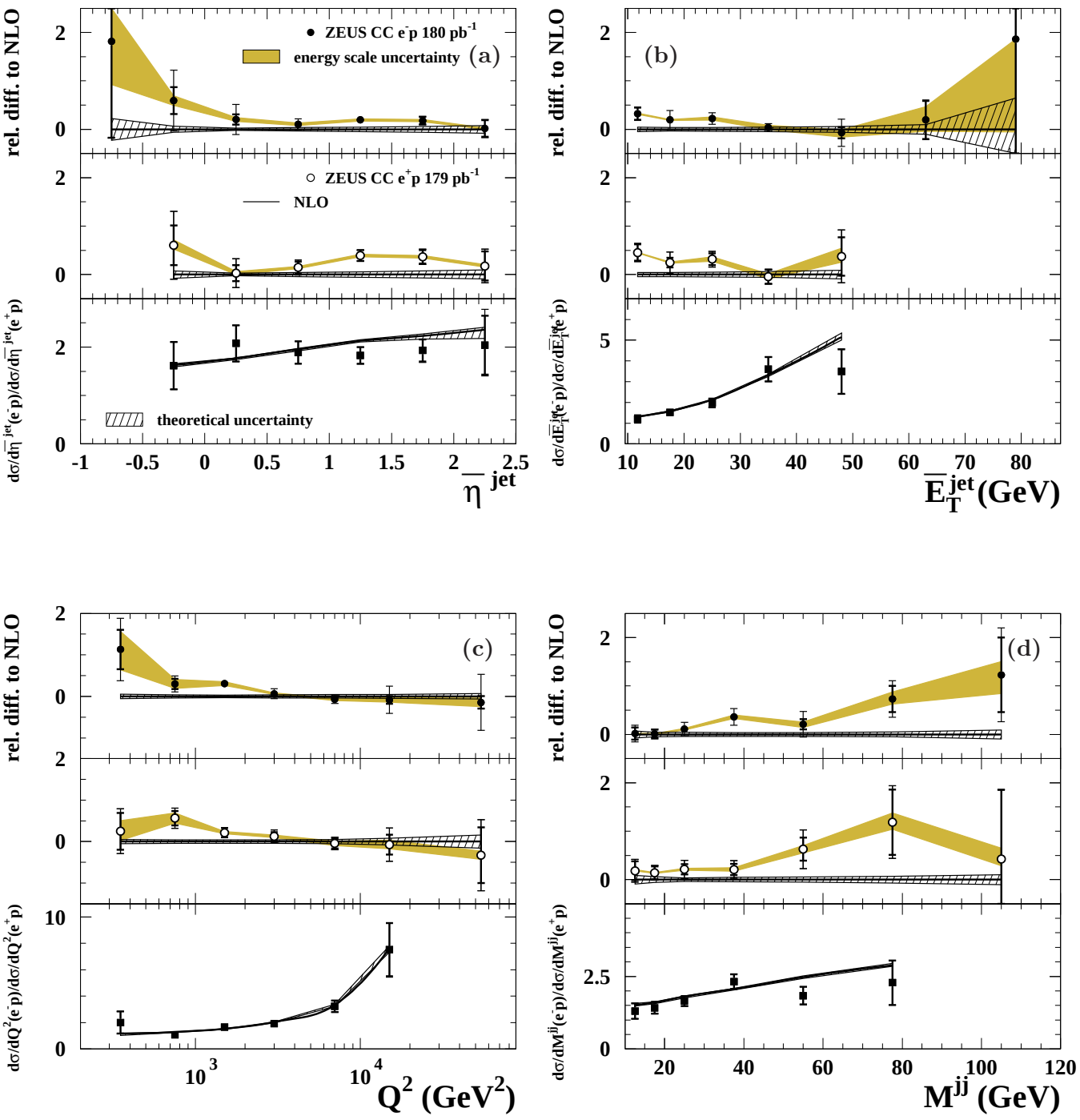

Figure 11: *Relative difference between the measured cross sections of Fig. 10 and the corresponding NLO QCD predictions in e^-p (dots) and e^+p (open circles) collisions as functions of (a) $\overline{\eta}^{\rm jet}$, (b) $\overline{E}_T^{\rm jet}$, (c) Q^2 and (d) $M^{\rm jj}$. The lower parts of the figures display the ratio of the cross sections for e^-p and e^+p collisions (squares). Other details as in the caption to Fig. 8.*

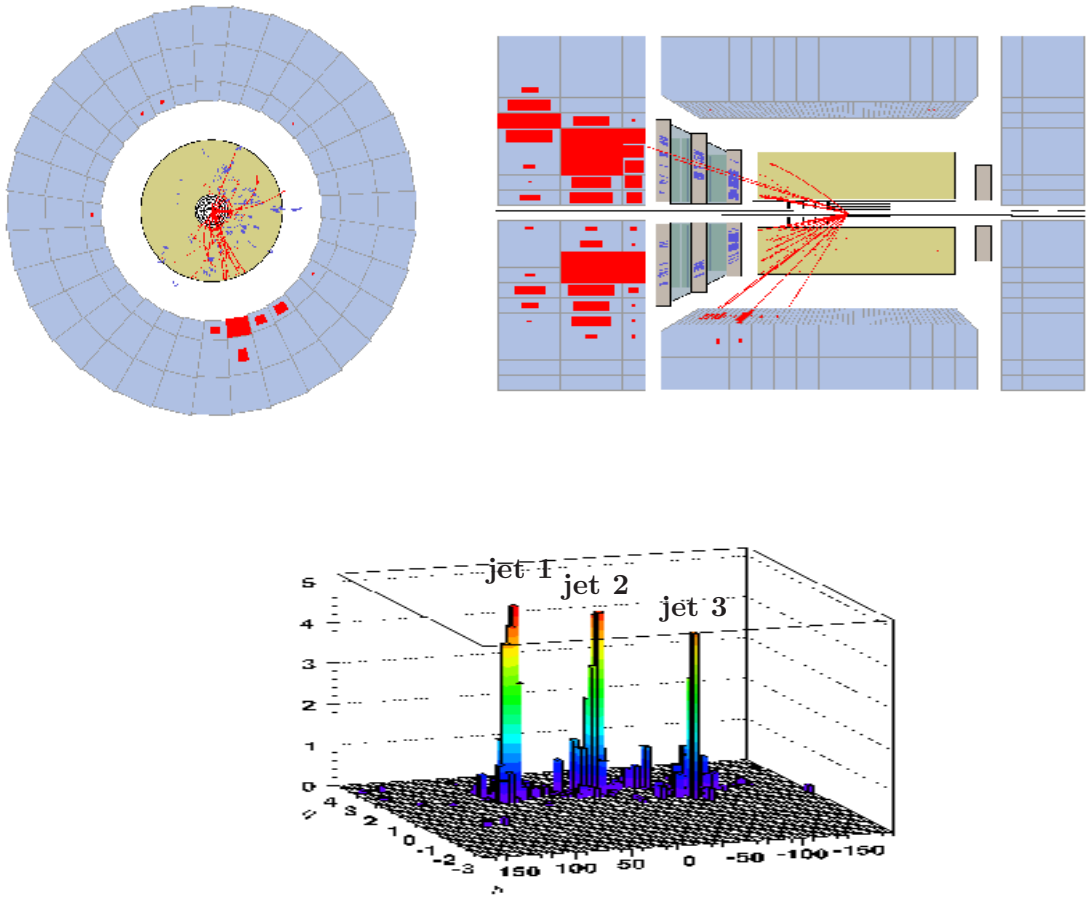

Figure 12: *Three-jet candidate event in CC DIS in the ZEUS detector. The energy deposition in the CAL is proportional to the size and density of shading in the CAL cells. The lego plots show the CAL transverse energy deposition projected in the $\eta - \phi$ plane. In the $X - Y$ view, only the energy deposition in the barrel calorimeter is shown.*

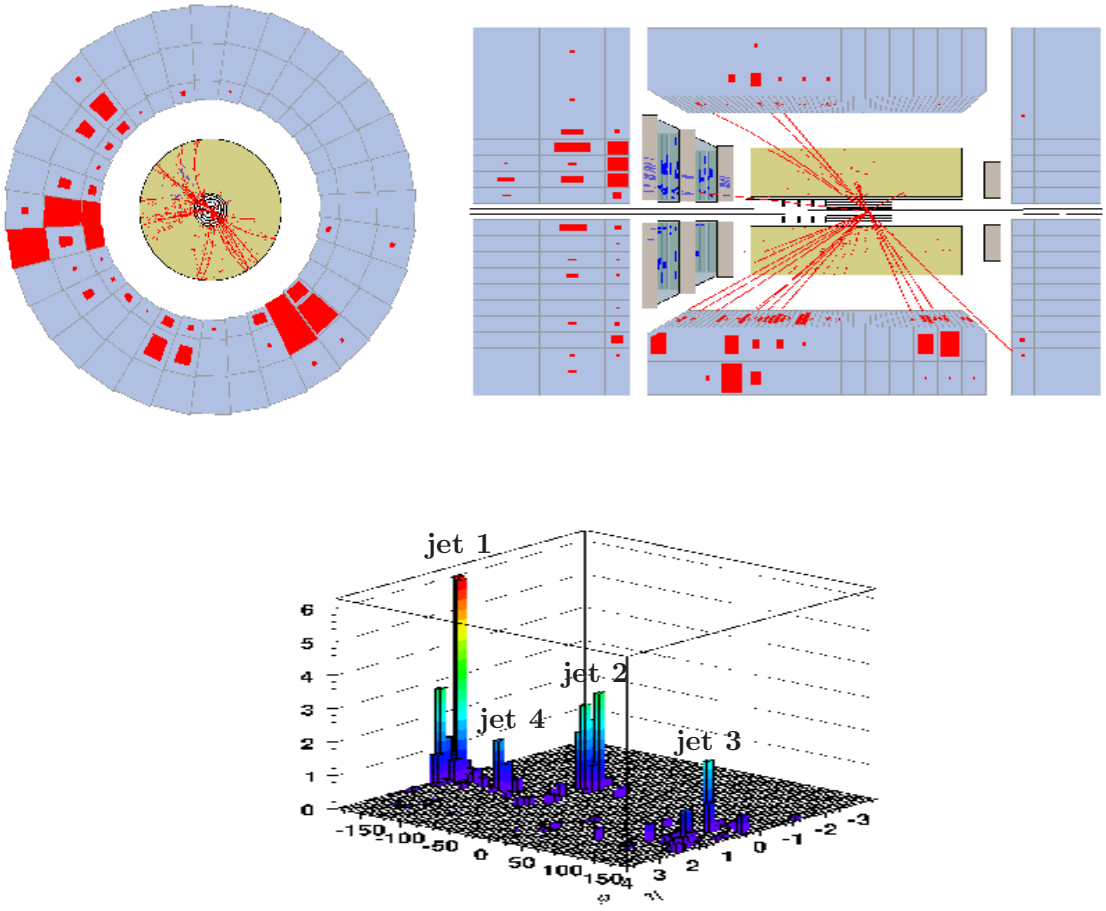

Figure 13: *Four-jet candidate event in CC DIS in the ZEUS detector. The energy deposition in the CAL is proportional to the size and density of shading in the CAL cells. The lego plots show the CAL transverse energy deposition projected in the $\eta - \phi$ plane. In the $X - Y$ view, only the energy deposition in the barrel calorimeter is shown.*

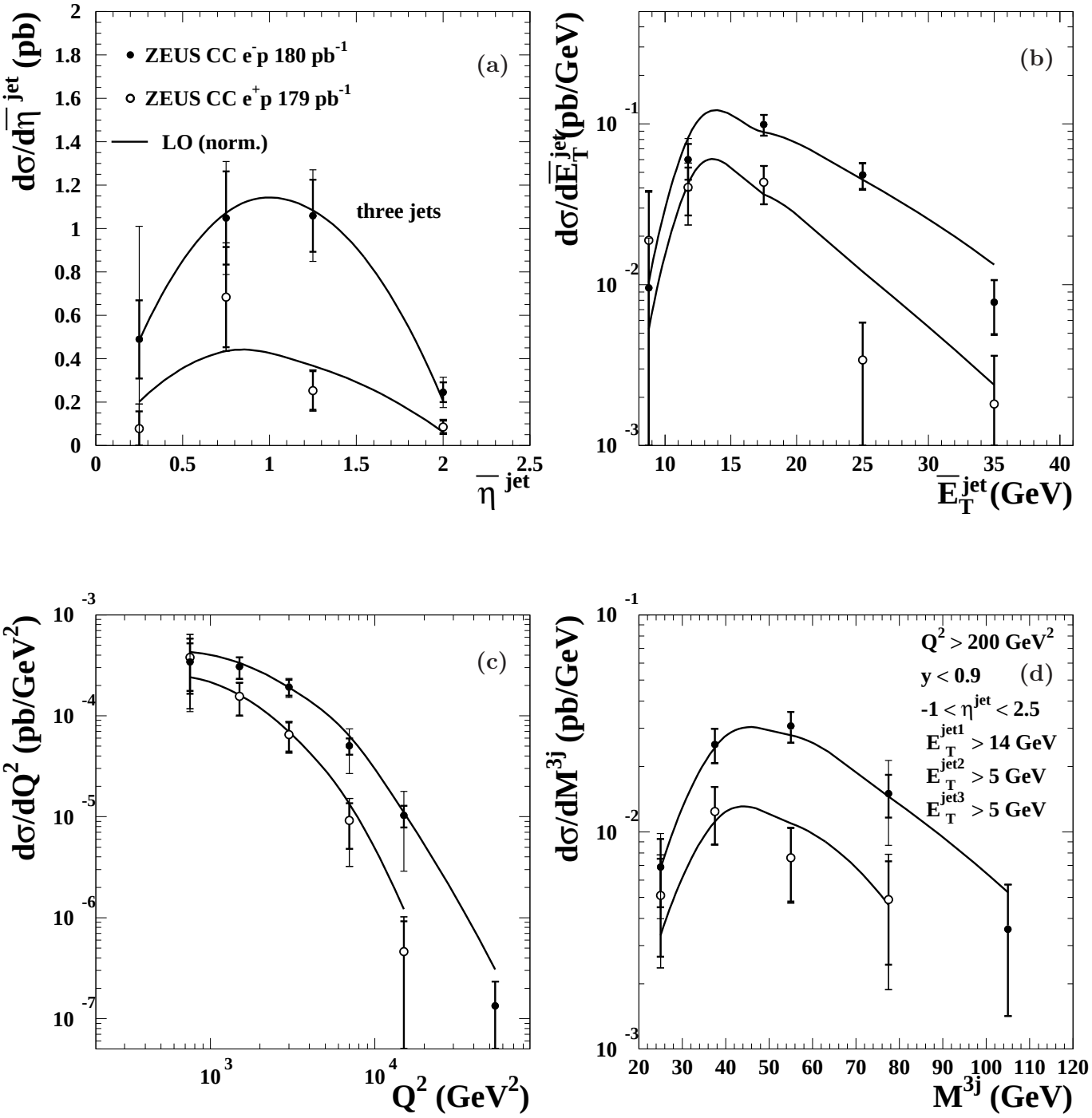

Figure 14: *Measured unpolarized three-jet cross sections in CC DIS for jets with* $E_T^{\rm jet1} > 14$ *GeV,* $E_T^{\rm jet2} > 5$ *GeV,* $E_T^{\rm jet3} > 5$ *GeV and* $-1 < \eta^{\rm jet} < 2.5$ *in the kinematic regime given by* $Q^2 > 200$ GeV^2 *and* $y < 0.9$ *as functions of (a)* $\overline{\eta}^{\rm jet}$, *(b)* $\overline{E}_T^{\rm jet}$, *(c)* Q^2 *and (d)* $M^{\rm 3j}$ *in* e^-p *(dots) and* e^+p *(open circles) collisions. For comparison, the predictions of LO QCD based on the* MEPJET *calculations using the ZEUS PDF sets (solid lines) are also shown. The predicted cross sections are normalized to the measured three-jet cross sections (*$\times 1.92$ *for* e^-p *and* $\times 1.42$ *for* e^+p*). Other details as in the caption to Fig. 7.*

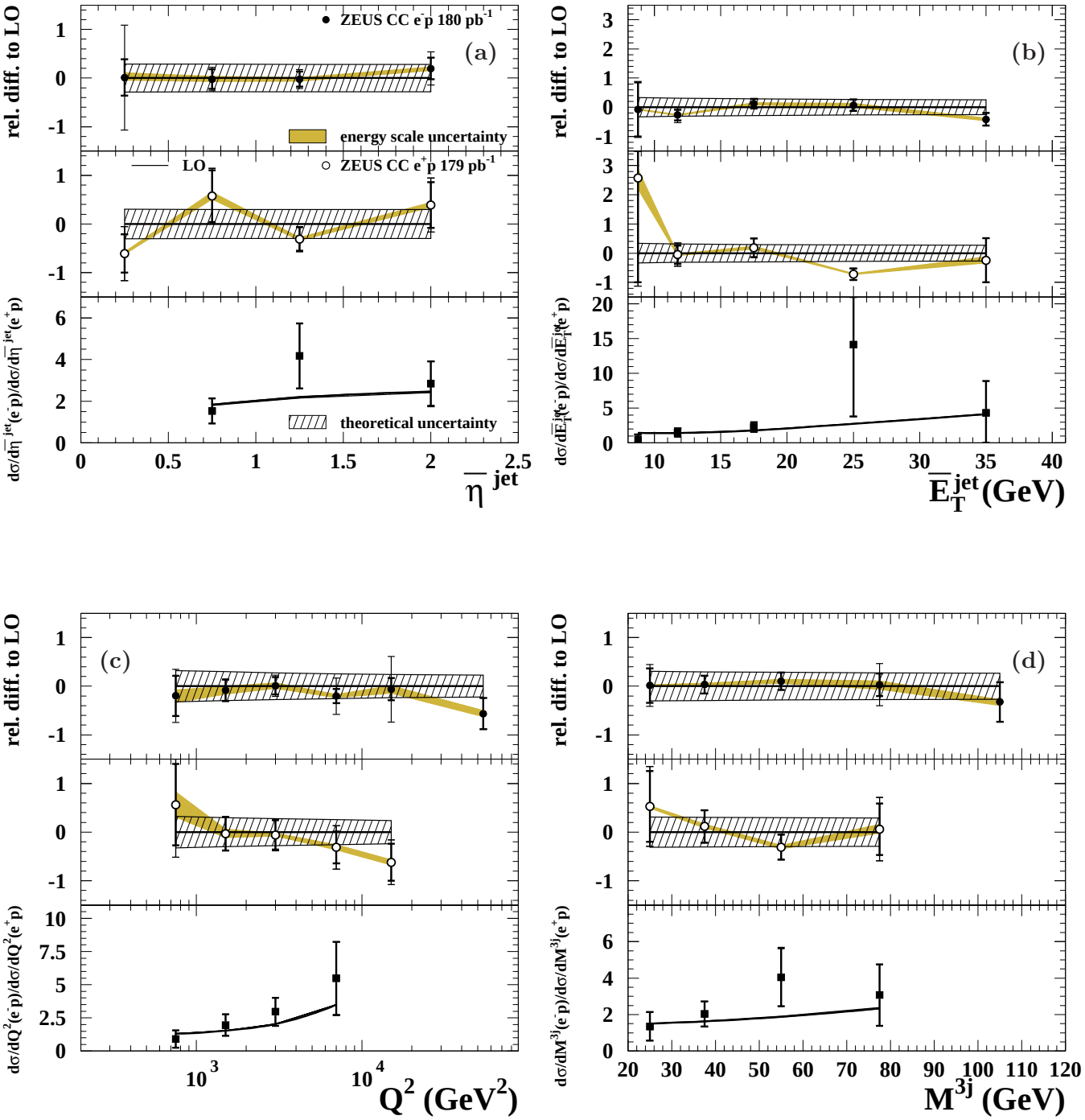

Figure 15: *Relative difference between the measured cross sections of Fig. 14 and the corresponding LO QCD predictions in e^-p (dots) and e^+p (open circles) collisions as functions of (a) $\overline{\eta}^{\rm jet}$, (b) $\overline{E}_T^{\rm jet}$, (c) Q^2 and (d) $M^{\rm 3j}$. The lower parts of the figures display the ratio of the cross sections for e^-p and e^+p collisions (squares). Other details as in the caption to Fig. 8.*